

1 **Retrotransposons facilitate the tissue-specific horizontal transfer of circulating tumor DNA**
2 **between human cells**

3

4 Munevver Cinar¹, Lourdes Martinez-Medina², Pavan K. Puvvula², Arsen Arakelyan³, Badri N.
5 Vardarajan², Neil Anthony⁴, Ganji P. Nagaraju⁵, Dongkyoo Park¹, Lei Feng², Faith Sheff⁶,
6 Marina Mosunjac⁶, Debra Saxe⁶, Steven Flygare⁷, Olatunji B. Alese¹, Jonathan Kaufman¹, Sagar
7 Lonial¹, Juan Sarmiento⁸, Izidore S. Lossos⁹, Paula M. Vertino¹⁰, Jose A. Lopez¹¹, Bassel El-
8 Rayes⁵, Leon Bernal-Mizrachi^{1*}.

9

10 ¹Department of Hematology and Medical Oncology, Winship Cancer Institute of Emory
11 University, Atlanta; ²Kodikaz therapeutic solutions, LCC, New York, NY; ³Bioinformatics group,
12 Institute of Molecular Biology NAS RA, Yerevan, Armenia; ⁴Departments of Integrated Cellular
13 Imaging Core, Winship Cancer Institute of Emory University, Atlanta, GA; ⁵Division of
14 hematology and oncology O'Neal Comprehensive Cancer Center, University of Alabama at
15 Birmingham, Birmingham, AL; ⁶Pathology and Laboratory Medicine, Winship Cancer Institute of
16 Emory University, Atlanta, GA; ⁷Department of Computational Biology/ Genetics, The University
17 of Utah, Salt Lake City, UT; ⁸Department of Surgery, Winship Cancer Institute of Emory
18 University, Atlanta, GA; ⁹Department of Medicine, Division of Hematology-Oncology and
19 Molecular and Cellular Pharmacology, Sylvester Comprehensive Cancer Center, University of
20 Miami, Miami, FL; ¹⁰Department of Biomedical Genetics and the Wilmot Cancer Institute,
21 University of Rochester Medical Center, Rochester, NY; ¹¹Bloodworks Northwest Research
22 Institute, Division of Hematology, University of Washington School of Medicine, Seattle, WA.

23

24 *Corresponding Author:

25 Leon Bernal-Mizrachi, MD

26 Winship Cancer Institute, Emory University

27 1365 Clifton Road, Building C, 3rd floor

28 Atlanta, GA 30322

29 Tel: 404-778-1839, Fax: 404 – 778-5520

30 lbernal@emory.edu

31 **Manuscript Information:** No. of words in Summary 266, Main text: 5819, Methods: 2578.

32 Number of Figures: 6, Number of Supplemental Figures: 5, supplemental tables 4. Supplemental

33 Videos: 3. Supplemental Method:1. Number of references: 53.

34

35

36

37

38

39

40

41

42

43

44

45

46

47 **Abstract**

48 A variety of organisms have been shown to have altered physiology or developed pathology due
49 to gene transfer, but mammals have never been shown to do so. Here, we show that circulating
50 tumor DNA (ct) can promote cell-specific horizontal gene transfer (HGT) between human cancer
51 cells and explain the mechanisms behind this phenomenon. Once ctDNA enters the host cell, it
52 migrates to the nucleus and integrates into the cell's genome, thereby transferring its genetic
53 information. We determine that retrotransposons of the ERVL, SINE, and LINE families are
54 necessary for cell targeting and the integration of ctDNA into host DNA. Using chemically
55 synthesized retrotransposons, we found that AluSp and MER11C reproduced multiple myeloma's
56 (MM) ctDNA's cell targeting and integration into MM cells. We also discovered that ctDNA
57 might, as a result of HGT, influence the treatment response of multiple myeloma and pancreatic
58 cancer models. Overall, this is the first study to show that retrotransposon-directed HGT can
59 promote genetic material transfer in cancer. There is, however, a broader impact of our findings
60 than just cancer since cell-free DNA has also been found in physiological and other pathological
61 conditions as well. Furthermore, with the discovery of transposons-mediated tissue-specific
62 targeting, a new avenue for the delivery of genes and therapies will emerge.

63

64

65

66

67

68

69

70

71

72

73

74

75

76

77 **Introduction**

78 The transfer of genes between cells is known to play an important physiological and pathological
79 role in many organisms. In prokaryotes, horizontal gene transfer (HGT) produces changes more
80 impactful in the genome evolution than the branched trajectory¹. Acquisition of novel traits
81 through HGT can provide prokaryotes with survival and evolutionary advantages against
82 environmental stressors^{2,3}. HGT in bacteria occurs by multiple molecular mechanisms. Among
83 them, conjugation and transformation take place through mobile genetic elements such as
84 transposons^{2,4-7}.

85

86 The exchange of genetic material via transposons is a ubiquitous method for HGT in some
87 eukaryotes such as insects and plants. From the initial discovery of transposon-mediated genetic
88 exchange between rice and millet plants⁸, much evidence of transposon-mediated HGT has been
89 detected in plants, particularly parasitic plants. Acquisition of the host plant's genetic material
90 allows parasitic plants to evolve more rapidly to adapt to new and changing environments. In fact,
91 on many occasions, the exact moment of transposon-mediated HGT defines the branch point in
92 the evolution of different versions of the invasive plants⁹. Similar events of transposon-mediated
93 HGT have been observed in drosophila.

94

95 In contrast to the examples above, the evidence in humans for HGT and any potential mechanism
96 involved are less well established. Under physiological conditions, a few studies have shown the
97 relocation of non-gene-coding regions between human cells^{10,11}. In immunology, early data
98 suggest that the exchange of cell-free DNA from a T cell can elicit the synthesis of antibodies by
99 B cells. In pathological conditions such as cancer, the evidence is even more rare. The discovery
100 that tumor-derived cell-free DNA can contain genetic alterations relevant to tumorigenesis¹² led
101 researchers over the last decade to evaluate the possibility that circulating tumor DNA (ctDNA)
102 serves as a vehicle for genetic exchange between tumor cells¹³. Their results suggest that HGT
103 can occur and alter tumor phenotype by transferring oncogenic genes or reshaping the tumor
104 microenvironment¹⁴⁻¹⁶. However, definitive evidence of ctDNA-mediated HGT and the
105 mechanism involved in HGT has been lacking until now.

106

107 In this study, we found that tissue-specific retrotransposons mediate the process whereby ctDNA
108 target and transmits genetic material to cells that resemble their cell of origin. These discoveries
109 lay the framework for a new field of study on the role of ctDNA in cell-cell communication and
110 its ramifications in fields such as embryogenesis, cell evolution, cancer, immunology, and
111 therapeutic gene transfer.

112

113 **Results**

114

115 **ctDNA incorporation into tumor cells resembling its cell of origin**

116 To determine whether ctDNA is capable of targeting cancer cell lines, we isolated ctDNA from
117 the plasma of various patients with multiple myeloma (MM), metastatic pancreatic cancer (PC),
118 and colon cancer (CC). First, we verified that nucleic acids extracted from plasma were genomic
119 DNA by showing that DNase I digestion abolished the DNA signal on agarose gel but RNase A
120 or proteinase K did not (Supplemental Figure 1A). Next, we confirmed that the DNA found in the
121 circulation of these patients reflects the cancer patients' tumor genome. Comparisons of exon and
122 whole-genome sequencing from primary tumors and the ctDNA of PC and MM patients revealed
123 that 100% of the ctDNA mutations correspond to the tumor mutational landscape, but roughly
124 20% of the tumor mutations cannot be identified by ctDNA sequencing. These results confirm that
125 ctDNA was produced by tumor cells (Supplemental Figure 1B). Based on these findings, we set
126 out to evaluate the possibility that ctDNA targets cancer cells and is capable of translocating into
127 the nucleus. To do so, we introduced rhodamine-labeled ctDNA from patients with MM [n=4],
128 pancreatic [PC, n=3], colon [CC, n=3], and lung cancer [LC, n=1] into the culture media of cell
129 lines that matched the ctDNA's tumor tissue of origin. The ctDNA localized in the nucleus of all
130 of the corresponding tumor cell types (Figure 1A, Supplemental Video 1A and B) at different
131 levels compared to the control signal of cells alone. We validated this observation using flow
132 cytometry; more than half of multiple myeloma cells (MM1s:52-54%) and almost all pancreatic
133 cancer (MIA: 99%) and colon cancer (HCT116:99%) cells were in contact with ctDNA (Figure
134 1B). However, after removing plasma membrane-bound ctDNA with trypsin, only 20-30% of the
135 MM1 cells and almost all MIA (99%) and HCT116 (99%) cells remained positive for Cy5 labeled
136 ctDNA. These startling results demonstrate the efficiency of ctDNA in transferring genetic
137 material between tumor cells.

138

139 To validate that ctDNA can enter cells, we used monoclonal antibodies against double-stranded
140 DNA (dsDNA) extracted from patients with systemic lupus erythematosus (SLE) that bind to
141 specific DNA sequences ¹⁷, which we hypothesized would disrupt the interaction of double-
142 stranded ctDNA with a potential cell membrane receptor. We cultured ctDNA isolated from MM
143 and PC patients overnight with two different anti-dsDNA antibodies. Subsequently, the ctDNA-
144 antibody mixtures were exposed to cells for 24 hours. Anti-dsDNA antibodies significantly
145 decreased rhodamine-labeled ctDNA signals in the nucleus (ctDNA nuclear intensity: 3.23-4.2
146 MM and 2.06-2.8 PC) compared to the IgG isotype control (16.5MM ctDNA and 25.6 PC,
147 p0.0001, Figure 1C) or PBS (7.9 MM and 14 PC). To corroborate the capacity of ctDNA to
148 transport and integrate non-orthologous genetic material into target cells, we ligated a linearized
149 CMV-Green Fluorescent Protein (GFP) vector into the middle of a ctDNA fragment of a myeloma
150 patient and added the product to MM1s cells in culture. We detected a GFP signal in cells cultured
151 with the ctDNA-containing CMV-GFP construct, whereas cells cultured with CMV-GFP alone
152 did not show a GFP signal (Supplemental Figure 1C). These data provide further evidence that
153 ctDNA can mediate HGT between cancer cells.

154

155 Next, we investigated the time required for ctDNA to enter the nucleus in multiple myeloma and
156 pancreatic cancer cell lines. In the pancreatic cancer cell line ASPC-1, ctDNA from a PC patient
157 targeted the cell membrane within seconds, internalized into the cytoplasm within minutes, and
158 localized into the nucleus within 10 minutes (Figure 1D and Supplemental Video 2A-C). In
159 contrast, ctDNA from a multiple myeloma patient reached the cell membrane of MM1s cells within
160 2 hours, internalized into the cytoplasm within 6 hours, and reached the nucleus within 8 hours,
161 with a maximum nuclear localization at 24 hours (Figure 1D).

162

163 **ctDNA preferentially migrates to tumor cells in mice**

164 To test *in vivo* the hypothesis that ctDNA targets tumor cells, we developed xenograft models
165 using PC (MIA), MM (MM1s), and CC (HCT-116) cell lines. In a pilot study using a PC xenograft,
166 we injected rhodamine-labeled PC ctDNA or PBS (control) into the tail of the mice. Results
167 determined that the maximum tumor localization of rhodamine-labeled ctDNA was detected at 48
168 hours post-tail vein injection (Supplemental Figure 1D). We then tested the tumor localization

169 using ctDNA from different cancer patients. Rhodamine-labeled ctDNA isolated from patients
170 with multiple myeloma, pancreatic cancer, and colon cancer (n=3 per tumor type) were injected
171 into the tail-vein of mice bearing the corresponding tumor xenografts (n=3 per tumor type). Mice
172 bearing the same type of tumors were injected with rhodamine alone (n=2) as a control. Tumors
173 and organs (liver, spleen, lung, kidney, colon, and pancreas) were harvested 48 hours after
174 injection, and frozen sections were prepared. Confocal microscopy using a red channel identified
175 a high rhodamine signal in the tumors of mice injected with rhodamine-labeled ctDNA compared
176 to control mice (Figure 1E). No immunofluorescence signal was detected in any organs examined,
177 suggesting that ctDNA preferentially accumulates in tumor cells (Supplemental Figure 1E).

178

179 **ctDNA is predominantly incorporated into cells from the same cell of origin**

180 The observation that ctDNA preferentially targets tumor cells raises the possibility that ctDNA has
181 a selective tropism for cells similar to those from which the ctDNA originated. We tested this
182 possibility by coculturing ctDNA with tumor cell lines from tissues distinct from the patient
183 ctDNA tissue of origin. When ctDNAs derived from PC or CC patients were cultured with MM
184 cell lines, the ctDNA clustered on the periphery of the cell membrane and failed to internalize. We
185 observed a similar phenomenon in experiments in which PC and CC cell lines were cocultured
186 with ctDNA extracted from mismatched-tumor-type patient plasma. On the other hand, ctDNA's
187 nuclear internalization was significantly increased when ctDNA was cocultured with cells
188 matching the ctDNA's tumor type (Figure s 2A and B). We validated this unexpected finding by
189 simultaneously adding ctDNA from patients that matched or did not match the tumor type of MM
190 (MM1s and JK6L), PC (PANC1 and ASPC-1), and CC (HT29 and HCT-116) cell lines and
191 measuring the nuclear localization of the ctDNA. The ctDNA only accumulated in the cell nucleus
192 if it originated from a patient whose tumor matched the cell line's tissue of origin (Figure 2C and
193 D). Otherwise, the ctDNA remained at the cell exterior. Finally, 3D reconstruction of the images
194 allowed us to identify that in the infrequent events in which mismatched ctDNA migrated into the
195 nucleus, it colocalized with matching ctDNA (Supplemental Video 3A and B).

196

197 We then studied whether ctDNA displayed cell-specific tropism *in vivo* in 2 xenograft models
198 (MM and PC). Rhodamine-MM and CY5-PC-labeled ctDNA were simultaneously injected into
199 the tail veins of each animal (n=2). Microscopy of the tumors demonstrated that rhodamine-ctDNA

200 from MM patients accumulated more in MM xenografts than in PC xenografts. In contrast, CY5-
201 labeled PC ctDNA accumulated in the PC xenograft but not in MM xenografts (Supplemental
202 Figure 1E). These data demonstrate that *in vivo* as *in vitro*, ctDNA selectively targets cancer cell
203 types similar to its cell of origin.

204

205 **Chromosomal integration of ctDNA**

206 We carried out metaphase chromosomal spreads of MM, PC, and CC cell lines after they were
207 cocultured with ctDNA matching the tumor cell type (N=3 per tumor type) to test if ctDNA
208 fragments are capable of integrating into the cell genome. Data showed rhodamine-ctDNA bands
209 incorporated in multiple chromatids (Figure 3A and Supplemental Figure 2A). The number of
210 chromatids with integrated ctDNA appears to vary depending on the cell line (Figure 3B).

211

212 The capacity of ctDNA to integrate into the genome was further defined using DNA repair
213 inhibitors. Myeloma (MM1s), pancreas (ASPC-1), and colon (HCT 116) cancer cells were treated
214 for 2 hours with the inhibitors of DNA damage response (i.e., ATM inhibitor (KU-55933), DNA-
215 dependent protein kinase catalytic subunit inhibitor (DNA-PK inhibitor II), and an inhibitor of
216 alternative join repair, such as poly (ADP-ribose) polymerase (PARP, NU1025)]. Following
217 treatment with these inhibitors, ctDNA was added to the culture medium, and chromosome spreads
218 were performed 24 hours later. Inhibition by the ATM and DNA-PKcs inhibitors significantly
219 reduced the integration of ctDNA into the genome compared to untreated cells. In contrast, PARP
220 inhibition had little effect on ctDNA integration in most cells (Figure 3C and Supplemental Figure
221 2B). These results could not be explained by changes in the viability of the cells after treatment
222 with the different inhibitors (Supplemental Figure 2C). Overall, these data further demonstrate the
223 capacity of ctDNA to integrate into the host cell genome and suggest cellular pathways that
224 mediate ctDNA 1ntegration/ligation.

225

226 These results prompted us to analyze the ctDNAs sequences integrated into the cell genome. We
227 performed a comparison analysis of whole-genome sequences from 2 cell lines, MM1s (multiple
228 myeloma) and MIA (pancreatic cancer) cell lines, ctDNA from the patients used to generate the
229 data in Figure 3B, and cell lines after being cocultured for 24 hours with the isolated ctDNA. First,
230 we evaluated whether single nucleotide variants (SNVs) unique to the ctDNA could be identified

231 in the coculture condition. Nucleotide variants were identified by comparing the sequence from
232 each experimental condition after alignment to the reference human genome (Hg38). Multiple
233 SNVs were identified in common between coculture conditions and ctDNA that were not present
234 in the genome of the untreated control cells (here called "SNVs of interest," Figure 3D). Further
235 detailing of these SNVs of interest demonstrated that cells cocultured with ctDNA showed skewing
236 of the variant allele frequency towards that of the variant ctDNA allele compared to cells alone
237 (Figure 3E). Further examples of SNVs exhibiting ctDNA 'skewing' in the variant allele frequency
238 (VAF) after coculture with ctDNA are shown in Figure 3F and Supplemental Figure 3A.

239

240 Next, we used the sequence data to reconstruct genomic contigs for each experimental condition
241 by de novo assembly. Comparison analysis of the contig sequences between the cell line, ctDNA,
242 and coculture condition indicated that ctDNA fragments were integrated into the cell genome
243 under coculture conditions. Blast analysis further validated the gain of ctDNA fragments in
244 coculture conditions and identified the transition points of ctDNA insertion (Figure 3G and
245 Supplemental Figure 3B). Thus, these orthogonal analytical approaches confirm the introduction
246 of ctDNA fragments into the cell genome under coculture conditions. Analysis of incorporated
247 ctDNA fragments and genome-insertion sites identified from both tumor models indicated that
248 most (~67%) of the inserted ctDNA fragments originated from chromosomes 3 and 7. Moreover,
249 80% of the ctDNA fragments targeted cellular chromosomal regions near the genomic location
250 from which ctDNA originated (Supplemental Spreadsheet 1). The remaining 20% were inserted
251 into a chromosomal location distinct from their site of origin. These findings are consistent with
252 the higher genetic recombination rate between homologous regions ^{18,19}.

253

254 Next, we explored whether inserting the ctDNA fragments enriched any particular pathway. Due
255 to the small number of insertions, the gene ontology analysis of the tissue-specific inserted
256 segments failed to attain statistical significance (Supplemental Figure 4). Gene ontology analysis
257 of the tissue-specific inserted fragments failed to reach significance due to the low number of
258 insertions utilized (Supplemental Figure 4). However, several trends of pathways enriched by MM
259 and PC inserted fragments. The phosphatidylinositol metabolic process, microtubule and
260 calmodulin binding, double-stranded RNA binding, and mitochondrial protein-containing
261 complex were among the enriched pathways in MM. The pathways for cell junction assembly, cell

262 morphogenesis regulation, cell cortex, histone deacetylase complex, and protein tyrosine
263 phosphatase activity, among others, tended to be enriched in PC inserted pieces (Supplemental
264 Figure 4).

265

266 **Retrotransposons are located at the 5' and 3' ends of the inserted ctDNA fragments**

267 Transposable elements (TE) play an essential role in HGT in prokaryotes and a few eukaryotes
268^{20,21}. Hence, we designed experiments to identify the presence of transposons in ctDNA fragments.
269 To map ctDNA genomic junctions more precisely, we ligated a PACBIO probe to multiple
270 myeloma and pancreatic cancer ctDNA samples to label their 5' and 3' ends. We then performed
271 whole-genome sequencing using the Illumina platform. De novo assembly was performed on the
272 sequencing output. ctDNA contigs containing the PACBIO adaptor were then matched to those
273 contigs containing inserted ctDNA sequences identified in the coculture experiments.
274 RepeatMaster²² detected and classified the transposable element on ctDNA sequences at the
275 insertion points (<100 nucleotides from transition point between cell and ctDNA)²². This analysis
276 demonstrated that the ctDNA fragments integrated into the cell genome contained more
277 transposable elements than non-integrated ctDNA fragments (Supplemental Table 1). These
278 findings suggest that retrotransposons mediate horizontal gene transfer in cancer cells, as they do
279 in prokaryotes and plants.

280

281 Next, we searched for transposons that preferentially target cells of matching tumor types. Hence,
282 we compared the list of transposons identified at the ctDNA insertion point in matching and
283 mismatching coculture conditions (i.e., MM ctDNA and MM cells or PC cells) and selected
284 transposons that were uniquely inserted in the matching conditions. Interestingly, class I
285 transposons, ERV-Ls, LTRs, SINEs, and LINEs, comprised the majority of transposable elements
286 at the transition points in pancreatic cancer or multiple myeloma. Within matching PC ctDNA,
287 AluSx, MIRc, and MTL1J were some of the most common retrotransposons subfamilies located
288 at insertion points. In multiple myeloma, AluSp, MER11, MER11C, AluJb, and L2a, among other
289 subfamilies of retrotransposons, were identified at the MM ctDNA insertion sites (Figure 4A and
290 Supplemental Table 2).

291

292 Activation of short interspersed nuclear elements (SINEs) and long interspersed nuclear elements
293 (LINE) has been observed in cancer, leaving open the possibility of retrotransposition. We,
294 therefore, evaluated the expression of transposable elements in RNA from cancer cells from 60
295 MM and 23 PC patients. To this end, batch normalized raw data was used to measure the
296 expression variability (methods section). The analysis confirmed several tissue-specific
297 retrotransposons to be highly expressed across pancreatic cancer or multiple myeloma. These
298 findings demonstrate that the retrotransposons identified at insertion sites were being transcribed
299 in these cancer types (Figure s 4B and C).

300
301 To evaluate the role of retrotransposons in horizontal gene transfer of ctDNA, we analyzed the
302 impact of inhibiting reverse transcription or integrases on ctDNA integration. Therefore, before
303 adding the ctDNA to the culture media, we treated the multiple myeloma (MM1s), pancreatic
304 cancer (MIA), and colon cancer (HCT116) cell lines with the reverse-transcriptase inhibitors
305 zidovudine (AZT) or didanosine (DDI), as well as with the integrase inhibitor raltegravir ²³. When
306 compared to the no-treatment control, the use of the reverse transcriptase and integrase inhibitors
307 significantly decreased ctDNA chromatid integration (Figure 4D and Supplemental Figure 2A),
308 giving proof that retrotransposons are crucial for ctDNA integration into the host cell's genome.

309
310 **Chemically synthesized retrotransposons target cells of similar tumor origin.**
311
312 To determine if the retrotransposons identified above can transfer genetic material between cancer
313 cells, we chemically synthesized several MM retrotransposons containing point mutations unique
314 to the tumor type and tested their HGT capacity. To this end, we selected among the list of
315 retrotransposons those that can be synthesized via the gBlock gene fragment method (AluSp,
316 AluSg2, MER11C, THE1A, and AluSx). Before any cell line experiment, we evaluated whether
317 they were able to resist degradation by DNases present in complete culture media. A synthetic
318 sequence with similar length and GC content that does not encode a retrotransposon and a PC
319 retrotransposon (AluSx1) were used as controls. Agarose gel electrophoresis demonstrated that all
320 fragments remain intact under culture conditions (Supplemental Figure 5A). Following these
321 results, we labeled these retrotransposons with CY5 and evaluated their capacity to target and
322 internalize in MM cell lines. First, we evaluated the kinetics of retrotransposon capture by flow

323 cytometry. Our results showed that cell capture of CY5-AluSp increases over time more efficiently
324 than the capture of the control sequence (Supplemental Figure 5B). Subsequently, we performed
325 dose titration experiments to evaluate cell capture and internalization. We considered the DNA
326 internalized if it was not removed from the cells with trypsin treatment. Cell capture and
327 internalization CY5-AluSp were dose-dependent and more efficient than the capture of the control
328 sequence (Supplemental Figure 5C). Based on these findings, we compared the efficiency of cell
329 capture of all transposons in two MM cell lines at 4 hours of culture. CY5-AluSp and CY5-
330 MER11C were captured more efficiently than the other MM transposons, the control sequence, or
331 PC transposons (Figure 5A and Supplemental Figure 5D).

332

333 The cell targeting of AluSp and MER11C was then measured in bone marrow samples from
334 patients with multiple myeloma or without multiple myeloma but with other bone marrow
335 disorders. After 14 hours of culture with marrows derived from myeloma patients, we observed
336 more CY5-positive plasma cells (CD 38 [+]) in marrows cultured with CY5-AluSp or -MER11C
337 than with control or PC sequences (Figure 5B). In contrast, AluSp or MER11C did not exhibit a
338 difference in CD38 (-) cell capture compared to control or PC sequences. As further evidence of
339 their ability to specifically target malignant plasma cells, we found that AluSp and MER11C-CY5
340 capture was more effective in CD38 (+) cells than in CD38 (-) cells (AluSp CD38 [+]: 9.9% 1.6%
341 vs CD38 [-]: 5.2% 0.8% P=0.03 and MER11C: CD38 [+]: 16.50% 3.8 vs CD38 [-]: 7% 1.2% P=0.
342 032). However, there was no distinction between CD38 (+) and CD38 (-) cells in control or PC
343 sequence cell capture. Experiments with the bone marrow of non-myeloma patients demonstrated
344 a similar tendency of greater CD38 (+) cell capture by AluSp and MER11C compared to controls
345 or PC sequences, with the trend disappearing in CD38 (-) cells. Lastly, when we compare the
346 uptake of malignant CD38 (+) cells to non-malignant CD38 (+) cells, we see a non-significant
347 increase in the AluSp and MER11C uptake of malignant CD38(+) cells.

348

349 To test whether the retrotransposon sequence contains a cell recognition signal, we generated
350 several deletion mutants of the AluSp sequence and evaluated their impact on cell capture. As
351 shown in Figure 5C, deleting the 3' end of AluSp reduced MM cell capture, suggesting that the
352 last 230 based pairs contain an MM cell recognition sequence. Multiple sequence alignments
353 (MSA) of AluSp and all MM-specific transposons revealed several conserved nucleotides and two

354 GC and AT-rich regions towards the 3' end region (Supplemental Figures 5E and F). Having
355 determined that AluSp was able to target MM cells specifically, we evaluated whether it could
356 deliver other genetic material into cells. For this, we ligated AluSp sequences to both ends of a
357 linearized CMV-mCherry cassette. These AluSp-mCherry ligates were then added to the culture
358 media of MM1s cells for 24 hours, after which mCherry expression was evaluated microscopically.
359 More AluSp-mCherry–treated cells expressed mCherry than cells incubated with the linearized
360 vector or the circular CMV-mCherry vector (Supplemental Figure 5G). Flow cytometry also
361 detected mCherry expression in MM1s cells (Figure 5D). To determine whether the mCherry
362 cassette integrated into the MM1s genome, we sequenced the genomes of single cells expressing
363 different levels of mCherry. mCherry insertions were identified by recognizing sequences with
364 one read aligned to the cell genome while the mate aligned to the CMV-mCherry sequence. This
365 analysis detected various mCherry insertions in cells with mid or high expression levels, while no
366 insertions were identified in cells without mCherry expression (Figure 5E). In contrast, when cells
367 were cultured with control-mCherry sequence, only a few were found with high levels of mCherry
368 insertion and expression. mCherry integration was confirmed by mCherry PCR of cells cultured
369 with AluSp-mCherry vector but not control-mCherry cultured cells (Figure 5F). The AluSp-CMV-
370 mCherry vector integrated high confidence into two specific regions in the genome
371 (Chr2:32916224-32916626 and Ch16:32628381-32629000), which are enriched for simple
372 repeats and AluSp, respectively (Figure 5G).

373

374 After demonstrating that AluSp can deliver a gene, we investigated whether this property can be
375 exploited therapeutically. We ligated a herpes simplex virus thymidine kinase (HSV-Tk) killer
376 gene between AluSp sequences (AluSp-HSV-Tk-GFP) and tested this vector's ability to kill MM,
377 PC, and CC cell lines. Cells were cultured for 24 hours with the AluSp-HSV-Tk-GFP and then
378 cultured for 96 hours in ganciclovir (GCV). At that point, we measured the effect on cell numbers
379 of the biologically active byproduct of GCV produced by the action of HSV-Tk. As shown in
380 Figure 5H, GCV markedly reduced the viability of MM cells previously treated with MM-AluSp-
381 HSV-Tk. In contrast, AluSp-HSV-Tk/GCV treatment did not affect the viability of PC or CC cell
382 lines. These results demonstrated that the synthetic AluSp could transfer and integrate genetic
383 cargo into specific cells (Figure 5H).

384

385 **ctDNA alters the drug response of MM or PC cell lines.**

386 Having demonstrated horizontal gene transfer in cancer cells, we explored potential consequences
387 of transfer on the phenotype of target cells, including on the target cell's response to drugs. We
388 therefore cultured Bortezomib-sensitive (BS) MM cell lines (MM1s and OPM1) for 24h with
389 DNase-treated or non-treated serum from bortezomib-resistant (BR) patients or control serum from
390 non-cancer patients. Subsequently, increasing doses of bortezomib were added to culture media,
391 and cell survival was measured 24 hours later. Compared to control plasma, plasma from patients
392 resistant to bortezomib increased the bortezomib resistance of MM1s and OPM1 (Figure 6A). This
393 effect of BR plasma was eliminated by pretreating with DNase (Figure 6A). When BR MM cell
394 lines (JK6L and RPMI) were cultured with a plasma of patients sensitive to bortezomib, the cells
395 exhibited a significant restoration of bortezomib sensitivity compared to when the cell lines were
396 cultured with control plasma. DNase treatment of BS plasma abolished this effect to levels similar
397 to control plasma (Figure 6B). Similar experiments were performed with PC cell lines (MIA Paca-
398 2 [MIA] and PANC1) using DNase-treated gemcitabine (GEM)-resistant (GR) and control plasma.
399 Both cell lines became resistant to GEM when cultured with GR plasma but not with control
400 plasma. DNase-treatment of the GR plasma abrogated the effect (Figure 6C). In contrast, DNase
401 treatment of control plasma resulted in increased resistance of PC cells to gemcitabine (Figure 6C,
402 lower graphs).

403

404 To further characterize the contribution of ctDNA transferring drug response, we added cell-free
405 ctDNA from bortezomib-resistant or -sensitive patients to media containing plasma of a patient
406 without cancer or BR. The plasma was then incubated with MM1 or OPM1 cells. Both cell types
407 lost sensitivity to bortezomib (Figure 6D). Resistance to bortezomib was increased even further
408 when the cells were incubated with the plasma of a BR patient to which BR patient ctDNA had
409 been added (Figure 6D). In contrast, adding the ctDNA of a BS patient to RPMI cells cultured with
410 control plasma from a non-cancer patient resulted in increased sensitivity to bortezomib (Figure
411 6D). These findings suggest that ctDNA transmits genes that confer drug sensitivity or resistance
412 from one cell to another.

413

414 **Discussion**

415 Horizontal transmission of TEs plays a significant role in the evolution of prokaryotes and some
416 eukaryotes. However, the role of HGT in humans has not been clearly described. We have
417 discovered that naked ctDNA can serve as a vehicle for transferring genes between cancer cells.
418 Beyond defining the fundamentals of ctDNA HGT, we discovered a previously unknown feature
419 of ctDNA: its preference for cells that are similar to those from which it originated. The
420 identification of retrotransposons at ctDNA insertion sites, the reduction of ctDNA insertions by
421 inhibitors of retrotransposition, and the results showing that synthetically-generated
422 retrotransposons can deliver payloads to target cells support the notion that retrotransposons have
423 an essential role in mediating HGT in cancer. Furthermore, our experiments using deletion mutants
424 of the retrotransposon delineated that these elements contain the address that specifies the delivery
425 of ctDNA to a specific target cell. Importantly, these results are laying the groundwork for research
426 into the use of a synthetic Transposon-mediated Gene Transfer (TGet) to precisely transfer "cargo"
427 to particular cells.

428

429 There is limited data available in humans to suggest that some cells transfer information through
430 the release of naked double-stranded DNA^{11,24}. Two groups have explored the role of ctDNA as a
431 messenger of genetic material in cancer *in vivo* models over the last decade^{11,14,15}. Garcia-Olmo
432 and colleagues suggested that plasma from colon cancer patients is capable of promoting tumor
433 development in a murine embryo fibroblast cell line (NIH-3T3). More importantly, this team
434 showed that plasma from CC patients transmitted oncogenes, including K-Ras, into NIH-3T3 cells
435^{15,25}. These findings were later supported by Trejo-Becerril and colleagues, who observed the
436 transfer of the human K-Ras oncogene from SW480 xenograft to chemically-induced colon cancer
437 tissue in rats¹⁴. These results align with our studies demonstrating the transfer of genetic material
438 from a patient's plasma to cancer cell lines. We demonstrated that ctDNA integrates into host cells
439 using whole-genome sequencing, GFP expression in cells cocultured with a ctDNA-CMV-GFP
440 cassette, and mCherry integration in cells treated with ctDNA-derived retrotransposons. Thus, we
441 provide solid evidence that ctDNA functions as a vehicle for gene transfer and is consistent with
442 our hypothesis that ctDNA can play a role in altering the genetic architecture of the tumor mass.
443 More importantly, our observations demonstrating the tissue-specific tropism of ctDNA provide a
444 potential mechanistic explanation for the studies of Trejo-Becerril¹⁴, which showed the transfer
445 of mutated human K-RAS from colon cancer cell lines grafted in mice carrying

446 dimethylhydrazine-induced colonic tumors. However, our data falls short of identifying the
447 mechanisms by which ctDNA binds cells and is internalized. Hence, further work elucidating the
448 cellular mechanism for ctDNA recognition will be essential for developing inhibitors to prevent
449 the transmission of genetic material between cancer cells as a means of spreading drug resistance.

450

451 The mechanism by which cell-free DNA transfers information between tumor cells has remained
452 elusive^{14,15}. The evidence that HGT in bacteria, flies, and plants is primarily mediated by specific
453 mobile elements²⁶ suggested the possibility that a similar mechanism occurs between cancer cells.
454 We uncovered multiple lines of evidence for the central role of retrotransposons in ctDNA HGT:
455 1) genomic analysis identified the presence of retrotransposons at insertion sites and their
456 expression in tumor samples; 2) both integrase and reverse-transcriptase inhibitors reduced ctDNA
457 integration into host cells; 3) synthetic MM retrotransposons were captured by both MM cell lines
458 and plasma cells derived from patients, and 4) MM transposons were able to deliver and integrate
459 mCherry and HSV-TK genes into MM cell lines. Nevertheless, it remains unclear why transposons
460 can perform tissue-specific HGT. The process of retrotransposition is known to be reactivated in
461 cancer cells^{27-30 47}. Thus, it is conceivable that upon arrival at the host cell, a particular transposon
462 carried by ctDNA co-opts the cellular retrotransposition machinery to integrate into the cancer cell
463 genome. Hence, their tissue-specific integration may be determined by the retrotransposon's
464 sequence and the host's expression of the retrotransposition machinery²⁸.

465

466 Cell-free DNA is incorporated into immune complexes in SLE, serving as an antigen recognition
467 signal³¹. Specifically, a DNA sequence within the immune complex is what immune cells and
468 antibodies recognize^{32,33}. In an analogous fashion, our work suggests that a particular sequence
469 within the retrotransposon serves as a recognition signal for target cancer cells. Indeed, we
470 demonstrated that pretreatment of ctDNA with SLE antibodies reduces the number of cells
471 capturing labeled ctDNA in MM and PC cell lines. Furthermore, we demonstrated that a synthetic
472 Alu sequence targets and delivers cargo into tumor cells and that deletion of the 3' end of the Alu
473 disrupts cancer cell targeting, highlighting that certain retrotransposons contain a cell-targeting
474 signal. However, not every ctDNA fragment is captured by the target cell, suggesting that the
475 recognition sequence is not present in each ctDNA fragment. We proved this by demonstrating
476 that different retrotransposons identified at insertion sites displayed variable cell targeting

477 efficiency in MM. These findings together highlight the presence of specific sequence signals that
478 define the tropism for cell targeting, here called “zip code sequence.”

479

480 Our experiments showing that pretreating cells with trypsin prevent the cellular uptake of ctDNA
481 and that trypsin treatment after culturing the cells with ctDNA reduces the number of ctDNA-
482 positive cells strongly suggest the presence of a plasma membrane protein receptor for the cell-
483 targeting sequence. This putative receptor remains unidentified. Hence, this work generates new
484 questions to be addressed, including identifying consensus sequences for cell targeting,
485 determining which genetic and phenotypic characteristics of the target cell regulate recognition by
486 ctDNA, and identifying the membrane protein receptor(s) for ctDNA.

487

488 The high efficiency by which 2 of the MM transposon sequences target plasma cells while largely
489 sparing other bone marrow cells opens the possibility of exploiting these transposons as therapeutic
490 vectors. Similar to our demonstration of specific delivery of HSV-Tk into MM cells, these
491 transposons could also deliver drugs, radioisotopes, nanoparticles, or killer genes.

492

493 Given the genetically instability of cancer cells, we were surprised by the frequency with which
494 the ctDNA fragments were inserted into homologous chromosomal locations. It is known that
495 accurate replication and repair of DNA ensure the proper functioning of a cell. Mechanisms such
496 as homologous recombination play a vital role in this process, particularly between regions with
497 identical sequences ³⁴. Therefore, ctDNAs would be expected to highjack this machinery to
498 integrate in genomic regions corresponding to those from which they originated. Hence, the
499 sequence of the ctDNA can, to a substantial degree, define the directionality of insertion.

500

501 The relevance of HGT in cancer is unknown. Our data demonstrating that ctDNA derived from
502 patients changes the drug response phenotype of a cell line is somewhat surprising. The possibility
503 of transmitting cancer through blood transfusion is a controversial subject of investigation. In 2007
504 a large study from Scandinavia (n=888,843) of cancer-free transfusion recipients demonstrated an
505 increased rate of cancer development in years after transfusion compared to the expected incidence
506 rate ^{35,36}, suggesting the possibility that certain blood units contain substances that promote the
507 development of occult cancers. Similarly, other studies have demonstrated an increase in cancer

508 incidence after transfusion; however, the specificity of particular cancer remains a matter of
509 discussion ³⁷. Although some studies indicate that transfusion has immunosuppressive effects and
510 the presence of cytokines that can cause carcinogenesis ³⁸, it is likely that ctDNA in some
511 transfused units could potentially promote cancer development.

512

513 In summary, we report horizontal gene transfer between human cells capable of altering the
514 phenotype of recipient cells. The mechanism involves the secretion of the transposon and
515 accompanying genomic DNA from donor cells into the extracellular space from where it
516 eventually reaches the blood. From the blood, the ctDNA can reach the target cell, which is usually
517 a cell of the same tissue origin as the donor cell. On the target cell, a membrane receptor (likely a
518 protein) recognizes a specific address sequence in the transposon region of the ctDNA and
519 internalizes the ctDNA. The ctDNA travels to the nucleus and becomes integrated into the genome,
520 usually in a region homologous to the site of ctDNA origin, in a mechanism involving reverse
521 transcriptase and integrases. This is the first definitive report of horizontal gene transfer between
522 human cells, and the work raises at least as many questions as it answers. Yet to be determined are
523 the mechanism of ctDNA secretion, the nature of the specific receptor on the target cell, the
524 mechanism of internalization, the cGAS-cGAMP-STING host response ³⁹, and other mechanistic
525 aspects. Our findings also raise the possibility that genetic information can be transferred between
526 individuals, through blood transfusion, for example. Finally, the ability to specifically target
527 certain tumor cells potentially adds a powerful new weapon to treat cancer and other diseases.

528

529 **Methods**

530 **Clinical specimens and sample preparation**

531 We obtained retrospective plasma samples from 10 multiple myeloma (MM), ten pancreatic
532 cancer (PC), three colon cancer (CC), and two lung cancer (LC) patients from samples stored in
533 the Tissue and Acquisition Bank of the Winship Cancer Institute of Emory University. All patients
534 provided written informed consent approving the use of their samples under Institutional Review
535 Board approval. The ten patients with newly diagnosed MM were treated with bortezomib-
536 containing regimens (among them were five responders and five non-responders). Of the ten PC
537 patients, seven with advanced staged cancer were treated with gemcitabine (at the time of obtaining
538 the plasma sample, two patients were in partial response, and five had progressive disease), and

539 three early-stage patients had undergone surgical resection. Response in MM was determined
540 using the International Uniform Response Criteria for Multiple Myeloma, and PC patients were
541 evaluated using the Response evaluation criteria in solid tumors (RECIST) criteria. Plasma was
542 isolated after centrifuging blood samples at 1500 rpm for 10 minutes. The plasma supernatant was
543 collected for storage. Plasma from non-cancer patients was purchased from Innovative Research,
544 MI.

545
546 Bone marrow samples for the coculture of transposons were obtained from fifteen MM patients at
547 various statuses of the disease (four newly diagnosed, three patients post-bone marrow transplant,
548 and eight patients at relapse) and five patients without myeloma (2 patients newly diagnosed with
549 myelodysplastic syndrome, two patients post-treatment of acute myeloid leukemia and one patient
550 with diffuse large b cell lymphoma without marrow involvement)

551
552 **Cell lines and reagents**
553 The following cell lines were grown in Roswell Park Memorial Institute (RPMI) 1640 medium:
554 Four multiple myelomas (OPM1, RPMI, JK6L, and MM1S); one PC (ASPC-1); and one LC
555 (A549). Colon cancer cell lines (HCT-116 and HT-29) were cultured in McCoy media. Pancreatic
556 cancer cell lines (PANC1 and MIA Paca-2 [MIA]) were cultured in DMEM media, and CC cell
557 line RKO was cultured in EMEM. All culture media were supplemented with 10% fetal bovine
558 plasma, 1% L-glutamine, one mM sodium pyruvate, and 50 µg/ml penicillin-streptomycin. In MIA
559 cells, 2.5% horse serum was also added to the culture medium.

560
561 Bortezomib, gemcitabine, ganciclovir, and DNaseI were purchased from Sigma-Aldrich. RNase
562 A, 4, 6-diamidino-2-phenylindole (DAPI), CellLight Plasma Membrane-GFP, Bacman 2.0, and
563 Platinum Polymerase High Fidelity PCR Kit were purchased from ThermoFisher-Scientific. DNA-
564 PK inhibitor II and Raltegravir were purchased from Santa Cruz Biotechnology, KU-55933 (ATM
565 kinase inhibitor) from Selleckchem, and NU1025 (PARP inhibitor VI) from Calbiochem. Quick
566 Ligation Kit was purchased from New England Biolabs. Proteinase K, QIAamp MinElute ccfDNA
567 Kits protocol, and QIAamp DNA Blood Mini Prep Kit were purchased from Qiagen. Cell TiterBlue
568 Cell Viability Assay Kit was purchased from Promega. Label IT Cx-Rhodamine and Cy5 were

569 purchased from Mirus Bio. pLenti-III HSVtk Lentivirus vector was purchased from Applied
570 Biological Materials (abm).

571

572 **Cell viability**

573 Cell viability assays were performed in 96 well, black, clear-bottom microplates. For MM cell line
574 studies, 3×10^4 cells were cultured for 24 hours with media containing 10% human plasma of a
575 bortezomib resistant or -sensitive patient or a control non-cancer patient. Cells were then cultured
576 for 24 hours with titrating concentrations of bortezomib (doses: 0, 5, 10, 15, 50 nM, , Sigma). For
577 PC cell line viability studies, 1×10^4 cells were incubated for 24 hours with media containing plasma
578 of a gemcitabine-resistant patient or non-cancer patient. Subsequently, titrating concentrations of
579 gemcitabine (doses: 0, 10, 25, 50, 100, 200 μ M, Sigma-Aldrich, MO) were added to the culture
580 media, and cells were then incubated for 96 hours. CellTiter-Blue Cell Viability Assay was used
581 to evaluate cell viability according to the manufacturer's instructions (Promega). Cell viability was
582 measured by a fluorescent protocol in a microplate reader. Experiments were performed in
583 triplicate of 3 independent studies.

584

585 **ctDNA extraction and immunofluorescence labeling**

586 Isolation of ctDNA was performed following the QIAamp MinElute ccfDNA Kits protocol
587 (Qiagen, Cambridge, MA). The ctDNA was fluorescently labeled with either Cx-rhodamine or
588 CY5 using the Label IT[®] Nucleic Acid Labeling kit (Mirus Bio LLC, WI).

589

590 **Image acquisition**

591 One $\times 10^6$ cells cultured in 1 ml of culture media were incubated with rhodamine- or CY5-labeled
592 DNA at different time points. The methodology used to perform immunofluorescence in
593 suspension cell culture was conducted as previously described^{40,41}. Adherent cells (2.5×10^5 cells)
594 were grown on a coverslip prior to processing. After cells were attached to slides, slides were
595 washed with PBS twice, and the cells were then counterstained with 4, 6-diamidino-2-
596 phenylindole (DAPI) for nuclear detection (ThermoFisher MA). For live-cell imaging, the plasma
597 membrane was labeled following the cellLight Plasma Membrane-green fluorescent protein
598 (GFP), Bacman 2.0 protocol (ThermoFisher MA). The presented images are from triplicate

599 experiments. Images were acquired using a Leica SP8 LIGHTING confocal microscope housed in
600 the Cell Imaging and Microscopy Shared Resource, Winship Cancer Institute of Emory University.

601

602 Lattice light-sheet microscopy was used to obtain live images and movie acquisition presented in
603 Supplemental Videos 1-3. Images were acquired using a 3i v1 Lattice Light Sheet microscope in
604 sample scanning mode, with Δs of 0.8 μm and 71 steps, and a 20 μm x-dither scan of the lattice
605 pattern created with a 0.550 outer NA / 0.500 inner NA annuli. Volume data were collected using
606 a Hamamatsu ORCA-Flash 4.0 v2 via a Semrock FF01-446/523/600/677 blocking filter for both
607 488 nm and 560 nm laser channels (5% and 10% power, respectively) every 3 mins for 1 -2 hours.
608 Raw data was deskewed using 3i SlideBook 6 software to create correctly orientation volumetric
609 data. The 3D visualization, surfaces, and movies were created in Bitplane Imaris 9. Isosurface
610 settings were user selected for each dataset to represent signal boundaries efficiently.

611

612

613 **Nuclear localization quantification and image analysis**

614 For quantification of the nuclear localization of rhodamine- or Cy5-ctDNA, we obtained 10 images
615 per sample in fields with a minimum of 10 cells. Volumetric data sets were acquired using a Leica
616 SP8 confocal microscope. All data were acquired with the same x, y, and z sampling and with the
617 same xy zoom. Z-stack total heights were varied to encapsulate the thickness of the randomly
618 selected field of view. Data were analyzed using Fiji ²⁴, ilastik ²⁵, and Matlab computational
619 software (MathWorks Inc, MA). A Fiji macro was used to convert raw.lif files as required; ilastik
620 machine learning models were trained and then applied to classify specific nuclear morphologies;
621 and Matlab was used to process resulting probability maps and quantify rhodamine- or Cy5-DNA
622 signal within the nuclei. Further information about image processing and quantification of the
623 ctDNA nuclear localization is available at GitHub repository

624 (https://github.com/nranthony/nuc_ctDNA_process). The nuclear intensity fold change value was
625 calculated by measuring the nuclear intensity produced by the rhodamine or Cy5 labeled ctDNA
626 over the background intensity of the nuclear signal in control cells.

627

628 **Chromosome spreads and ctDNA banding identification**

629 Rhodamine-labeled ctDNA from patients with MM (n=3), PC (n=3), and CC (n=3) was added to
630 culture media. Briefly, 1×10^6 cells cultured in 1.5 mL of medium were incubated with 1 μ g/mL
631 of rhodamine-ctDNA. At 24 hours, the cells were transferred to a 15 ml tube and incubated in
632 10mL of medium containing 15 μ L Colcemid (10 μ g/mL) at 37°C for 20 minutes before harvesting.
633 After centrifugation and media removal, cells were resuspended with 10 mL of pre-warmed
634 0.075M KCl and incubated at 37°C for 20 minutes. Two mL of fixative (3:1 methanol: acetic acid)
635 were added and incubated for 10 minutes before centrifugation and aspiration. Samples were then
636 resuspended in 10mL of fixative and incubated at room temperature for 10 minutes, followed by
637 2 additional washes with a fixative. Slides were prepared in a Thermotron chamber where
638 temperature and humidity were controlled for optimum metaphase spreading. Serial micro-
639 pipetting was performed, 3 μ L at a time, until at least 25 cells were visible per field at 20x
640 magnification. After drying slides at room temperature for 1 hour, nuclei were stained with DAPI
641 plus antifade reagent, and coverslips were applied to slides. Cytogenetic technicians performed the
642 readout. Ten to twenty metaphase nuclei were counted per experiment, with touching and
643 overlapping cells excluded. The number of chromosomes with integrated rhodamine bands was
644 counted.

645

646 **Assessment of ctDNA integration with non-homologous end-joining repair, the alternative 647 pathway, and transposase inhibitors**

648 To investigate the mechanisms involved in ctDNA integration into the chromosomes of MM1s,
649 ASPC-1, and HTC116 cells, 1×10^6 cells were treated with inhibitors of the non-homologous end-
650 joining (NHEJ) repair system. The inhibitors were ataxia-telangiectasia mutated (ATM) inhibitor
651 KU-55933 (10 μ M, Santa Cruz Biotechnology, TX) and the DNA-dependent protein kinase,
652 catalytic subunit (DNA-PKCS) inhibitor I (30 μ M, Sigma-Aldrich, MO). In addition, we used
653 inhibitors for alternative NHEJ repair pathways, also known as microhomology-end joining, such
654 as the poly ADP ribose polymerase (PARP) inhibitor NU1025 (200 μ M, Sigma-Aldrich, MO) and
655 the transposase inhibitor raltegravir (100nM, Sigma-Aldrich, MO). After 2 hours post-drug
656 treatment with inhibitors, rhodamine-labeled ctDNA was added to the culture media and incubated
657 for an additional 24 hours. Cell growth was then arrested, and chromosome spreads were
658 performed as noted above. The number of rhodamine-ctDNA integration sites for each cell was
659 determined by counting a minimum of 10 cells in metaphase. The ctDNA band integration

660 identification and integration counts was performed by personnel from the cytogenetic laboratory
661 of Emory University.

662

663 **Xenograft experiments**

664 Mice were housed in a clean facility with an ambient temperature of 65-75°F, 40-60% humidity,
665 and 12 light/12 dark cycles. All experiments included male and female animals. The protocols
666 followed were approved by the Emory University Institutional Animal Care and Use Committee
667 and compliant with ethical regulations for studies involving laboratory animals.

668

669 We performed pilot and validation xenograft studies to evaluate the accumulation of ctDNA in
670 tumors in mice. For the pilot time-course study, three mice bearing pancreatic cancer MIA cell
671 xenografts were generated by injecting 1×10^6 cells in the dorsum of J:NU (007850) outbred nude
672 mice. After tumors reached a volume of 0.5 cm, mice were assigned to a specific experimental
673 arm: 2 mice underwent tail vein injection with rhodamine-labeled ctDNA, and a third mouse
674 received a tail-vein injection with PBS as a control. Tumors from tail vein ctDNA-injected mice
675 were harvested 24 and 48 hours post-injection. For mice in the control group, the tumor was
676 harvested 48 hours post-injection. Based on the results of these experiments, we selected a harvest
677 time point of 48 hours post-injection. For the validation study, xenograft models were developed
678 using human-derived PC (MIA), MM (MM1s), and CC (HCT-116) cell lines. Following the pilot
679 study protocol, three mice per tumor xenograft were then dosed to assess tumor localization of
680 labeled ctDNA. At harvest time, tumors and selected organs (liver, lung, large bowel, pancreas,
681 and spleen) underwent frozen section dissection. Each slide was fixed with paraformaldehyde 4%
682 and stained with DAPI before mounting the coverslip.

683

684 **Whole-genome sequencing and Whole exon sequencing**

685 ctDNA was extracted from ten MM and ten PC patients using the methods described above. DNA
686 from CD138(+) cells and from cell lines used in *in vitro* experiments (MM1s and MIA) was
687 extracted using the Blood & Cell Culture DNA Mini Kit (Qiagen, MD). DNA from fresh frozen
688 paraffin-embedded pancreatic tumors was obtained using QIAamp DNA FFPE Tissue Kit Print
689 (Qiagen, MD).

690

691 After extraction, ctDNA was ligated to the PACBIO adaptor (GCGCTCTGTGTGCT) using the
692 ABM DNA Library Prep Kit for Illumina Sequencing (Applied Biological Materials Inc. Canada).
693 PACBio-labeled ctDNA and regular ctDNA were subjected to standard methods for library
694 preparation and sequencing using Illumina and Agilent protocols, respectively. Applied Biological
695 Materials Inc. prepared the libraries and performed whole-exon and -genome sequencing. The
696 average target coverage was 50X.

697

698 **Nucleotide variance concordance between tumor and ctDNA**

699 Quality Control and Alignment To Reference Genome: The raw sequence data was subjected to
700 quality control checks using FastQC
(<https://www.bioinformatics.babraham.ac.uk/projects/fastqc/>). Samples that failed the QC checks
701 were trimmed using BBDuk (<https://jgi.doe.gov/data-and-tools/bbtools/bb-tools-user-guide/bbduk-guide/>) in the adapter trimming mode for paired reads. The sequence reads were then
702 aligned to the human genome GRCh38 assembly
(https://www.ncbi.nlm.nih.gov/assembly/GCF_000001405.39) using the Falcon Accelerated
703 Genomics Pipeline (<https://github.com/falconcomputing/falcon-genome>). This is an accelerated
704 version of the GATK Best Practices Pipeline. Beginning with paired-end FASTQ sequence files,
705 the first step mapped the sequences to the reference. The resulting mapped BAM file was sorted
706 and duplicates marked. We ran the GATK 4.1.3 best practice somatic mutation pipeline with base
707 recalibration, with read orientation filtering to account for damage seen when using FFPE samples
708 and (<https://www.intel.com/content/dam/www/programmable/us/en/pdf/literature/wp/wp-accelerating-genomics-open1-fpgas.pdf>, <https://www.intel.com/content/www/us/en/healthcare-it/solutions/genomicscode-gatk.html> and
709 <https://pdfs.semanticscholar.org/e85d/4f927d91e9f25b7c20de71f91c78250771bb.pdf>).

710

711 Variant Calling And Annotation: Variant calling was done using VarDict
712 (<https://academic.oup.com/nar/article/44/11/e108/2468301>), a novel and versatile variant caller
713 for next-generation sequencing in cancer research. VarDict was chosen based on the
714 recommendations from Sandmann et al ⁴². We used an allele frequency threshold of 0.01. Variants
715 for 6 of the samples (for which a control samples were not available) were called in single sample
716 mode (<https://github.com/AstraZeneca-NGS/VarDict>). For the samples where controls were

722 available, paired mode was run in order to distinguish between somatic and germline variants. The
723 called variants were annotated using SnpEff (<http://snpeff.sourceforge.net/SnpEff.html>), which is
724 a variant annotation and effect prediction tool. We used SnpEff's pre-built GRCh38.86 database
725 for the annotations.

726

727 Analysis for concordance of ctDNA and primary tumor sample: Single nucleotide variant
728 concordance between ctDNA and corresponding tumor samples was analyzed using bcftools isec
729 (<http://samtools.github.io/bcftools/bcftools.html>) to obtain concordant variants.

730

731 **De Novo Assembly and identification of ctDNA tissue specific sequences.**

732 To identify insertion in the coculture conditions, we used two different approaches for assembling
733 the genome. In approach 1, reads from ctDNA (5 MM and 5 PC, cell lines, and cells cocultured
734 with matched and mismatched ctDNA samples were assembled using ABySS ⁴³ de novo
735 assembler. Before assembly, ct-DNA samples were 10x depth normalized with bbnorm [5]. The
736 best k-mer size for the assembly was predicted and selected with the KmerGenie tool ⁴⁴,
737 (<https://jgi.doe.gov/data-and-tools/software-tools/bbtools/>). In addition, ct-DNA samples used in
738 cell line cultured experiments (772 and P201812-2) were assembled without any read depth
739 normalization.

740

741 ctDNA contig-level assembly sequences from MM and PC samples were used for cluster analysis
742 with the aim of identifying tissue-specific sequences. cd-hit-est-2d was used to select contigs
743 specific for MM and PC ⁴⁵ with 95% of identity as a threshold. cd-hit-est-2d compared to sequence
744 datasets (data base 1 [db1]=MM and data based 2 [db2]=PC) and reports sequences that are not
745 similar in db2 as well as sequences that are similar between db1 and db2. Since we were interested
746 in MM- and PC-specific contigs, we performed cd-hit-est-2d twice: first, MM contig assemblies
747 were assigned as db2 (for MM-specific contigs), and then PC contig assemblies were assigned as
748 db2 (for PC-specific contigs).

749

750 In approach 2 whole-genome sequences (WGS) from ctDNA (5 MM and 5 PC, cell lines, and cells
751 cocultured with matched and mismatched ctDNA samples were used to assemble genomes using
752 SPAdes 3.12.0 ⁴⁶. Prior to de novo assembly, ct-DNA samples were 10x depth normalized with

753 bbnorm (<https://jgi.doe.gov/data-and-tools/software-tools/bbtools/>). The best k-mer size for the
754 assembly was predicted with the KmerGenie tool ⁴⁴. In addition, ct-DNA samples used in cell line
755 cultured experiments were assembled without any read depth normalization. After this step human
756 mitochondrial DNA was removed using 2 strategies. First, sequence data was aligned to human
757 genome build 38 with the Burrows-Wheeler aligner ⁴⁷ and mitochondrial specific reads were
758 removed. Second, sequence reads were assigned to human mitochondrial genome using Centrifuge
759 (<https://ccb.jhu.edu/software/centrifuge/manual.shtml>) and a custom database.

760

761 **Detection tissue specific insertions**

762 Approach 1. The first method aligned all cell line samples to the human reference genome(hg38)
763 with bwa-mem software (v 0.7.17) ⁴⁸. After the alignment step de novo insertions detection was
764 performed with the Pamir tool ⁴⁹. Pamir uses “one-end anchor” reads (i.e. one end is mapped while
765 the other is unmapped around the breakpoint location) and orphan reads (read pairs where none of
766 the ends can be mapped to the reference) to characterize the novel sequence contents and their
767 insertion breakpoints. Algorithm steps include de novo assembly, re-alignment, and clustering on
768 mentioned reads to generate contigs for putative novel insertions. Aligned BAM files for cell
769 culture sequences along with the hg38 genome reference were supplied to Pamir. The tool outputs
770 a VCF file with the sequence, location, and length of identified novel insertions.

771

772 To select cancer type-specific inserts, full-length contigs were converted to BLAST databases.
773 Then, insertions identified in the match-, mismatch- and no-culture samples for corresponding cell
774 line samples (MM1S or MIA) were blasted against the corresponding sample full-length assembly
775 contig database (MM ctDNA for MM1S cells and PC ctDNA for MIA cells). An insert was
776 considered cancer-specific if: 1) it was present in the matching coculture sample but not in
777 mismatch coculture and no-culture samples; 2) it was aligned to the corresponding ct-DNA sample
778 database with an identity at least 70% (to maximize hits for further processing).

779

780 To define if the selected unique contigs are present in all samples, we have created a BLAST
781 database for all samples and blasted the unique contigs against each database. The myeloma
782 database consisted of contigs from five MM patients; for pancreatic cancer the database consisted
783 of ten PC patients. Unique contigs from each cancer type were blasted against the corresponding

784 database. Then, we selected the contigs, with alignment length \geq 650bp and BLAST identity
785 $\geq 90\%$. As a result, we have defined the unique contig sets, which were present in all samples
786 belonging to one cancer type (MM1S - 14 contigs and MIA - 13 contigs). In the next step, we have
787 aligned contigs in all samples with the corresponding insertion, using MAFFT [10], and
788 constructed the consensus sequences.

789
790 Approach 2. For the second approach, we used NucDiff ⁵⁰ to identify subsequence repeats,
791 deletions, or novel insertions by comparing WGS assembled de novo. NucDiff uses NUCmer,
792 delta-filter, and show-snps programs from MUMmer ⁵¹ for comparing closely related sequences.
793 For both MM and PC, we made the following comparisons: a) MM ctDNA cocultured with MM
794 Cells with the MM cells' sequence; b) MM ctDNA sequence from the same patient used for the
795 coculture experiment with the MM cells' sequence; c) MM ctDNA cocultured with PC cells; d)
796 MM ctDNA with the PC cells sequence; and e) PC ctDNA coculture with PC cells with the PC
797 cells sequence, PC ctDNA sequence from the same patient used for the coculture experiment with
798 the PC cells, and PC ctDNA coculture with MM cells. For each comparison, we set the parameter
799 "minimum length of a maximal exact match" to 250 (-l) and the minimum cluster length to 200 (-
800 c) to optimize the running time and detect large structural differences between the genomes.

801
802 The "struct.gff" and "snp.gff" output files from NucDiff was parsed to identify events that
803 represent transfer of DNA from the ctDNA sample to the cell in the coculture experiment. For
804 each event, we required a) minimum length of >100 base pairs, and b) that the structural event
805 identified with reference to a specific cell contig should be present in both the coculture and ctDNA
806 with an exact match of the insertion sequence with the ctDNA assembly. Inserted sequences from
807 the qualifying structural events in were aligned to the human genome build 37 using Bowtie2 ⁵² to
808 identify genomic co-ordinates of the ctDNA sequence that inserts into the cell. Genes that harbor
809 inserted ctDNA sequences were annotated using genomic co-ordinates from build 37 of the human
810 genome. Enrichment of gene-ontology pathways terms were tested in the identified genes using
811 the R clusterProfiler (<https://bioconductor.org/packages/release/bioc/html/clusterProfiler.html>).

812
813 **Identification of transposable elements and its nucleotide variants**

814 To determine the locations of transposable-like regions in the contigs, sequences were analyzed,
815 and transposable elements (TEs) were identified and classified using RepeatMasker version 4.1.0²²
816 and . The Dfam database (release 3.1⁵³) of repetitive DNA families was used as a reference for
817 identifying repeats in ctDNA contig sequences that were part of qualifying structural events as
818 described above. For each repeat sequence identified by RepeatMasker, we computed the overall
819 frequency of the specific repeat (e.g., for AluSp or L1) and their parent class (e.g., SINE).

820

821 Once the TE elements were identified, we aligned hit repeats/TE sequences, unique contigs for
822 all samples, and insertion sequence with MAFFT software version 7. Mutations in TE sequences
823 were identified by comparison of nucleotides at each position in the multiple sequence alignment
824 with the “Biostrings” R package (version 4.1). We considered a position to contain mutation if the
825 substitution was present in contigs of all samples. In the case of ambiguous nucleotides in contigs
826 introduced by short read alignment (putative heterozygosity in the sample), non-matched
827 nucleotide was considered as a mutation if it was present in all samples. Finally, based on the
828 identified mutations, we have constructed the mutated transposon sequences for each unique
829 contigs (for MM1S and MIA datasets).

830

831 **Transposon linearized vector**

832 A polynucleotide comprising sequences corresponding to the transposon that contained mutations
833 shared by all the MM samples was generated by Integrated DNA Technologies, Inc (IDT). The
834 sequence of these oligos are described in the supplemental methods section. Similar methods were
835 use to generate deletion mutants from AluSp.

836

837 **Statistical analysis**

838 Two side student-T test was use as statistical analysis method for evaluating the difference between
839 ctDNA nuclear localization among cell, the number of base gain in match and mismatch coculture
840 sequencing experiments, and the number of ctDNA integrations in chromatids under the different
841 experimental conditions. Statistical analysis for transposon enrichment was performed using Chi-
842 square test as noted above.

843

844

845 **Data Availability**

846 Sequencing data used for producing Figure 3C-D, 4B-C and Supplemental Figure 1B2 and 5A-D
847 is available under Figshare portal: <https://figshare.com/account/home#/projects/87485> .

848
849 For image processing and quantification of the ctDNA nuclear localization see GitHub repository
850 for the algorithms: https://github.com/nranthony/nuc_ctDNA_process.

851
852 **Acknowledgments**

853 We thank Dr. Ravi Majeti for their critical review and comments. LBM was supported by Georgia
854 Research Alliance venture development award. ISL is supported by grant 1R01CA233945 from
855 the National Cancer Institute, the DwoSkin, and Anthony Rizzo Families Foundations and Jaime
856 Erin Follicular Lymphoma Research Consortium. Research reported in this publication was also
857 supported in part by the Winship Shared Resource of Winship Cancer Institute of Emory
858 University and National Institutes of Health (NIH)/National Cancer Institute under award number
859 2P30CA138292-04. The content is solely the responsibility of the authors and does not necessarily
860 reflect the official views of the National Institute of Health. Also Imaging Core was supported in
861 part by PHS Grant UL1TR000454 from the Clinical and Translational Science Award Program,
862 National Institutes of Health, National Center for Advancing Translational Sciences.

863
864 **Author contributions**

865 CM: Conceived, planned and carried out the experiments, performed data analysis, and
866 participated in manuscript writing. B.N.V: developed the design, theory and performed the
867 computation analysis, also participated in manuscript writing. G.P.N, D.P: Conceived and planned
868 the *in vivo* experiments. F.S: Performed and analyzed all chromosomal-related experiments. S.F:
869 Performed Computational analysis. M.M, O.B.A, D.S: Contributed to sample preparation and data
870 analysis; I.S.L: contributed to the design of some experiments, interpretation of the results, and
871 writing the manuscript. J.K, S.L, J.S: Contributed to sample acquisition, data interpretation, and
872 writing the manuscript. B.E: Contributed to the design of some experiments, sample acquisition,
873 data interpretation and writing the manuscript. L.B-M: Conceived the original idea of the
874 manuscript, planned the experiments, contributed on the sample acquisition and approach for data

875 analysis, and interpretation of the results, and participated in manuscript writing. All authors
876 discussed the results and contributed to the final manuscript.

877

878 **References**

- 879 1. Bichsel, M., Barbour, A.D. & Wagner, A. The early phase of a bacterial insertion sequence
880 infection. *Theoretical Population Biology* **78**, 278-288 (2010).
- 881 2. Johnston, C., Martin, B., Fichant, G., Polard, P. & Claverys, J.-P. Bacterial transformation:
882 distribution, shared mechanisms and divergent control. *Nature Reviews Microbiology* **12**, 181
883 (2014).
- 884 3. Frost, L.S., Leplae, R., Summers, A.O. & Toussaint, A. Mobile genetic elements: the agents of
885 open source evolution. *Nature Reviews Microbiology* **3**, 722-732 (2005).
- 886 4. Wozniak, R.A.F. & Waldor, M.K. Integrative and conjugative elements: mosaic mobile genetic
887 elements enabling dynamic lateral gene flow. *Nature Reviews Microbiology* **8**, 552 (2010).
- 888 5. Gilbert, C. & Cordaux, R. Horizontal Transfer and Evolution of Prokaryote Transposable Elements
889 in Eukaryotes. *Genome Biology and Evolution* **5**, 822-832 (2013).
- 890 6. Cuecas, A., Kanoksilapatham, W. & Gonzalez, J.M. Evidence of horizontal gene transfer by
891 transposase gene analyses in *Fervidobacterium* species. *Plos One* **12**, e0173961 (2017).
- 892 7. Price, V.J., *et al.* Enterococcus faecalis CRISPR-Cas Is a Robust Barrier to Conjugative Antibiotic
893 Resistance Dissemination in the Murine Intestine. *mSphere* **4**, e00464-00419 (2019).
- 894 8. El Baidouri, M., *et al.* Widespread and frequent horizontal transfers of transposable elements in
895 plants. *Genome Res* **24**, 831-838 (2014).
- 896 9. Sun, T., *et al.* Two hAT transposon genes were transferred from Brassicaceae to broomrapes and
897 are actively expressed in some recipients. *Scientific Reports* **6**, 30192 (2016).
- 898 10. Huang, W., *et al.* Widespread of horizontal gene transfer in the human genome. *Bmc Genomics* **18**,
899 274 (2017).
- 900 11. Anker, P., *et al.* The role of extracellular DNA in the transfer of information from T to B human
901 lymphocytes in the course of an immune response. *International Journal of Immunogenetics* **7**,
902 475-481 (1980).
- 903 12. Schwarzenbach, H., Hoon, D.S.B. & Pantel, K. Cell-free nucleic acids as biomarkers in cancer
904 patients. *Nat Rev Cancer* **11**, 426-437 (2011).
- 905 13. Thierry, A.R., El Messaoudi, S., Gahan, P.B., Anker, P. & Stroun, M. Origins, structures, and
906 functions of circulating DNA in oncology. *Cancer Metastasis Rev* **35**, 347-376 (2016).
- 907 14. Trejo-Becerril, C., *et al.* Cancer Progression Mediated by Horizontal Gene Transfer in an In Vivo
908 Model. *Plos One* **7**, e52754 (2012).

909 15. García-Olmo, D.C., *et al.* Cell-Free Nucleic Acids Circulating in the Plasma of Colorectal Cancer
910 Patients Induce the Oncogenic Transformation of Susceptible Cultured Cells. *Cancer Research* **70**,
911 560-567 (2010).

912 16. Dvořáková, M., *et al.* DNA released by leukemic cells contributes to the disruption of the bone
913 marrow microenvironment. *Oncogene* **32**, 5201 (2012).

914 17. Jin, H., Sepúlveda, J. & Burrone, O.R. Specific recognition of a dsDNA sequence motif by an
915 immunoglobulin VH homodimer. *Protein Sci* **13**, 3222-3229 (2004).

916 18. Sung, P. & Klein, H. Mechanism of homologous recombination: mediators and helicases take on
917 regulatory functions. *Nature Reviews Molecular Cell Biology* **7**, 739-750 (2006).

918 19. Clancy, S. Genetic recombination. *Nature Education* **1**, 40 (2008).

919 20. Peccoud, J., Loiseau, V., Cordaux, R. & Gilbert, C. Massive horizontal transfer of transposable
920 elements in insects. *Proceedings of the National Academy of Sciences* **114**, 4721-4726 (2017).

921 21. Schaack, S., Gilbert, C. & Feschotte, C. Promiscuous DNA: horizontal transfer of transposable
922 elements and why it matters for eukaryotic evolution. *Trends in Ecology & Evolution* **25**, 537-546
923 (2010).

924 22. Smit, A., Hubley, R. & Green, P. RepeatMasker Open-3.0. . (<http://www.repeatmasker.org>) (1996-
925 2004).

926 23. Muşat, M.G., *et al.* HIV-1 integrase inhibitors targeting various DDE transposases: Retroviral
927 integration versus RAG-mediated recombination (Review). *Mol Med Rep* **20**, 4749-4762 (2019).

928 24. PB, G. & M., S. The virosome—a novel cytosolic informative entity and intercellular messenger.
929 *cell biochemistry and function* **28**, 529-538 (2010).

930 25. Bergsmedh, A., *et al.* Horizontal transfer of oncogenes by uptake of apoptotic bodies. *Proceedings
931 of the National Academy of Sciences* **98**, 6407-6411 (2001).

932 26. Emamalipour, M., *et al.* Horizontal Gene Transfer: From Evolutionary Flexibility to Disease
933 Progression. *Front Cell Dev Biol* **8**(2020).

934 27. Bogu, G.K., Reverter, F., Martí-Renom, M.A., Snyder, M.P. & Guigó, R. Atlas of transcriptionally
935 active transposable elements in human adult tissues. *bioRxiv*, 714212 (2019).

936 28. Chung, N., *et al.* Transcriptome analyses of tumor-adjacent somatic tissues reveal genes co-
937 expressed with transposable elements. *Mob DNA* **10**, 39 (2019).

938 29. Howard, G., Eiges, R., Gaudet, F., Jaenisch, R. & Eden, A. Activation and transposition of
939 endogenous retroviral elements in hypomethylation induced tumors in mice. *Oncogene* **27**, 404-
940 408 (2008).

941 30. Carnevali, D., Conti, A., Pellegrini, M. & Dieci, G. Whole-genome expression analysis of
942 mammalian-wide interspersed repeat elements in human cell lines. *DNA Res* **24**, 59-69 (2017).

943 31. Soni, C. & Reizis, B. DNA as a self-antigen: nature and regulation. *Curr Opin Immunol* **55**, 31-37
944 (2018).

945 32. An, Y., Raju, R.K., Lu, T. & Wheeler, S.E. Aromatic Interactions Modulate the 5'-Base Selectivity
946 of the DNA-Binding Autoantibody ED-10. *The Journal of Physical Chemistry B* **118**, 5653-5659
947 (2014).

948 33. Klecka, M., *et al.* Autoantibody Profiling in Lupus Patients using Synthetic Nucleic Acids. *Scientific Reports* **8**, 5554 (2018).

950 34. Probst, A.J. & Banfield, J.F. Homologous Recombination and Transposon Propagation Shape the
951 Population Structure of an Organism from the Deep Subsurface with Minimal Metabolism. *Genome
952 biology and evolution* **10**, 1115-1119 (2018).

953 35. Hjalgrim, H., *et al.* Cancer incidence in blood transfusion recipients. *Journal of the National
954 Cancer Institute* **99**, 1864-1874 (2007).

955 36. Goubran, H.A., *et al.* Impact of Transfusion on Cancer Growth and Outcome. *Cancer growth and
956 metastasis* **9**, 1-8 (2016).

957 37. Yang, T.O., Cairns, B.J., Reeves, G.K., Green, J. & Beral, V. Cancer risk among 21st century blood
958 transfusion recipients. *Annals of oncology : official journal of the European Society for Medical
959 Oncology* **28**, 393-399 (2017).

960 38. Cata, J.P., Wang, H., Gottumukkala, V., Reuben, J. & Sessler, D.I. Inflammatory response,
961 immunosuppression, and cancer recurrence after perioperative blood transfusions. *Br J Anaesth*
962 **110**, 690-701 (2013).

963 39. Cai, X., Chiu, Y.-H. & Chen , Z.J. The cGAS-cGAMP-STING Pathway of Cytosolic DNA Sensing
964 and Signaling. *Molecular Cell* **54**, 289-296 (2014).

965 40. Schindelin, J., *et al.* Fiji: an open-source platform for biological-image analysis. *Nat Methods* **9**,
966 676-682 (2012).

967 41. Berg, S., *et al.* ilastik: interactive machine learning for (bio)image analysis. *Nat Methods* **16**, 1226-
968 1232 (2019).

969 42. Sandmann, S., *et al.* Evaluating Variant Calling Tools for Non-Matched Next-Generation
970 Sequencing Data. *Scientific Reports* **7**, 43169 (2017).

971 43. Simpson, J.T., *et al.* ABySS: a parallel assembler for short read sequence data. *Genome Res* **19**,
972 1117-1123 (2009).

973 44. Chikhi, R. & Medvedev, P. Informed and automated k-mer size selection for genome assembly.
974 *Bioinformatics* **30**, 31-37 (2014).

975 45. Li, W. & Godzik, A. Cd-hit: a fast program for clustering and comparing large sets of protein or
976 nucleotide sequences. *Bioinformatics* **22**, 1658-1659 (2006).

977 46. Nurk, S., *et al.* Assembling single-cell genomes and mini-metagenomes from chimeric MDA
978 products. *J Comput Biol* **20**, 714-737 (2013).

979 47. Li, H. & Durbin, R. Fast and accurate long-read alignment with Burrows-Wheeler transform.
980 *Bioinformatics* **26**, 589-595 (2010).

981 48. Li, H. & Durbin, R. Fast and accurate short read alignment with Burrows-Wheeler transform.
982 *Bioinformatics* **25**, 1754-1760 (2009).

983 49. Kavak, P., *et al.* Discovery and genotyping of novel sequence insertions in many sequenced
984 individuals. *Bioinformatics* **33**, i161-i169 (2017).

985 50. Khelik, K., Lagesen, K., Sandve, G.K., Rognes, T. & Nederbragt, A.J. NucDiff: in-depth
986 characterization and annotation of differences between two sets of DNA sequences. *Bmc
987 Bioinformatics* **18**, 338 (2017).

988 51. Kurtz, S., *et al.* Versatile and open software for comparing large genomes. *Genome Biol* **5**, R12
989 (2004).

990 52. Langmead, B. & Salzberg, S.L. Fast gapped-read alignment with Bowtie 2. *Nat Methods* **9**, 357-
991 U354 (2012).

992 53. Hubley, R., *et al.* The Dfam database of repetitive DNA families. *Nucleic Acids Res* **44**, D81-89
993 (2016).

994

995

996 **Figure Legends**

997 **Figure 1. ctDNA incorporation into tumor cells.** A. Index images showing the nuclear
998 localization of rhodamine-labeled ctDNA (red) in multiple myeloma (MM1s) and lung (A549),
999 pancreatic (ASPC1), and colon (HCT116) cancer cell lines. The lower panel shows the box and
1000 whiskers plot summarizing fold change nuclear density derived from the comparison of cell lines
1001 cultured with ctDNA derived from patients with multiple myeloma (n=5), pancreatic (n=3), or
1002 colon (n=3) cancer and the background nuclear intensity of untreated control cells. Letters on the
1003 x-axis refer to individual patient samples. B. Flow cytometry assay demonstrated a high percentage
1004 of cells with ctDNA incorporation. One million myeloma (MM1s), pancreatic (MIA), and colon
1005 (HCT116) cancer cells were cultured with CY5-labelled ctDNA (1 μ g/mL) for 24 hours. To
1006 determine ctDNA internalization, cells were then treated for 30 minutes with trypsin (100 uL of
1007 0.25% Trypsin) to remove any ctDNA bound to membrane proteins. (Lower panel) Box plot
1008 summarizes triplicate experiments' data of each cell line cultured with multiple ctDNA samples
1009 derived from patient samples. Letters on the x-axis refer to individual patient samples. C. Anti-
1010 double stranded DNA antibodies (Anti-dsDNA) reduce ctDNA nuclear localization in multiple
1011 myeloma (MM1s) and pancreatic cancer (MIA) cells. Nuclear intensity density fold change of
1012 rhodamine-labeled ctDNA in cells after cultured with PBS (control), IgG (control), and anti-

1013 dsDNA antibodies from SLE patients 1 (SLE1) and 2 (SLE2). Images were taken 24 hours after
1014 coculturing antibody-ctDNA with cells. The nuclear signal was measured using similar methods
1015 as described in Figure 1A. D. Time course of cytoplasmic and nuclear localization of rhodamine-
1016 ctDNA from patients with pancreatic cancer and multiple myeloma in ASPC-1 (upper) MM1s
1017 (bottom) cells, respectively. In ASPC-1 cells, the membrane was labeled with GFP (green), and
1018 ctDNA was labeled with rhodamine (red). In MM1s cells time course, the nucleus was labeled
1019 with DAPI (blue) and ctDNA with rhodamine (red) E. Tumor localization of rhodamine-ctDNA
1020 and rhodamine alone (control) 48 hours after tail injection (representative images from triplicate
1021 experiments). Images in all samples were taken with an open red channel for rhodamine detection.
1022 MM: Multiple myeloma, PC: Pancreatic cancer, and CC: Colon cancer.

1023
1024 **Figure 2. ctDNA cell-specific targeting.** A. Index images of 10 experiments and B. fold change
1025 of ctDNA nuclear density measurements in cell lines cultured with ctDNA matching or not
1026 matching the patient's cancer type. B. whiskers plot summarizing fold change of nuclear density
1027 measurements of cells culture with ctDNA derived from cancer patients matching or not the tumor
1028 type of the cell line (n=10 experiments) C. Index images and (D) fold change of nuclear density
1029 measurements of simultaneous cocultured of tumor matched and unmatched ctDNA and cell lines
1030 (n=10 experiments). MM: multiple myeloma, CC: colon cancer, and PC: pancreatic cancer. MM
1031 cells: MM1S, RPMI, JK6L, PC cells: ASPC-1, PANC1, MIA, and CC cells: HT29 and HCT 116.
1032 Error bars in the box and whiskers plot identified the standard deviation of triplicate experiments.
1033

1034 **Figure 3. Integration of ctDNA is mediated by non-homologous end joining (NHEJ) repair**
1035 **and integrases.** A. Immunofluorescence index images of ctDNA (red) integration into chromatids
1036 (blue) in MM (MM1S), PC (ASPC-1), and CC (HCT116) cell lines. Circles define zoomed regions
1037 of interest. White arrows identify an area of ctDNA integration. B. Scatter plot displaying the
1038 number of chromatids with ctDNA integrations in different MM (MM1s, RPMI, OPM1), PC
1039 (MIA, PANC1, ASPC-1), and CC (HCT 116, HT29, RKO) cell lines. Error bars indicate standard
1040 deviations of triplicate experiments (n=20 metaphases per experiment). Color and symbol shapes
1041 signify different cell types. C. Incorporation of rhodamine-ctDNA fragments into chromosomes
1042 of multiple myeloma (MM1s), pancreatic cancer (ASPC-1), and colon cancer (HCT 116) cell lines
1043 after treatment with NHEJ (DNAPKcs and ATM), and PARP (n=10). Cells were pretreated for 2

1044 hours with inhibitors of DNA-PK (inhibitor II), ATM (KU-55933), and PARP (NU1025) before the
1045 addition of rhodamine-ctDNA to the cell culture. The number of integrated sites was measured in
1046 10-20 metaphases per condition. D. Gain of nucleotide variants in cells cocultured with ctDNA.
1047 Comparative SNV analysis between cell genome, ctDNA, and coculture. Venn diagram displays
1048 exclusive and shared SNVs between each experimental condition. The area marked in red
1049 highlights SNVs commonly shared between ctDNA and coculture condition ctDNA/cell. E.
1050 Stacked bar diagram demonstrating the changes in allele depth of the variant (red) and reference
1051 (Blue) allele in multiple myeloma ctDNA, cell line genome, and coculture condition. Cells under
1052 coculture conditions have more depth in the varian allele in several locations compared to the
1053 control cell genome. F. Figure s demonstrating two index IVG variant calls images and their allele
1054 frequency in multiple myeloma and pancreatic cancer experimental conditions. Green horizontal
1055 bars (Adenine) and blue (guanine) are, in these cases, the alternate nucleotide, and gray bars are
1056 the reference nucleotide. G. Blast images demonstrate the transition point of insertion between cell
1057 genome contigs (red boxes) and ctDNA contigs (green boxes). Results were obtained after
1058 comparing the contigs carrying insertions in the coculture condition with the reference cell
1059 genome. Coculture contigs carrying a ctDNA insertion were identified using NucDiff analysis.
1060 MM: Multiple myeloma, PC: Pancreatic cancer, and CC: Colon Cancer.

1061

1062 **Figure 4. Transposon-mediated horizontal gene transfer of ctDNA in cancer cells.** A. Tables
1063 summarizing the list of tissue-specific transposons identified at the ctDNA insertion sites. B.
1064 Expression levels of selected TE in PC and MM tumor samples. D. Scatter plot displaying the
1065 number of chromatid with rhodamine-ctDNA integration of MM (MM1s), PC (ASPC-1), and CC
1066 (HCT 116) cell lines (n=30) after treatment with two reverse transcriptase inhibitors (AZT and
1067 DDI) and an integrase inhibitor (raltegravir). Cells were pretreated, and analysis was performed
1068 using similar protocols as in Figure 3A. MM: Multiple myeloma, PC: pancreatic cancer, and CC:
1069 Colon cancer.

1070 **Figure 5. MM transposons mediated horizontal gene transfer to cancer cells.** A. MM1s cell
1071 capture an internalization of different multiple myeloma retrotransposons and controls after 4
1072 hours of culture. B. Index flow cytometry images displaying the cell capture of AluSp, MER11,
1073 PC transposon (AluSx) and control sequence in plasma cells and non-plasma cells derived from

1074 bone marrows of patients with newly diagnosed or treated multiple myeloma patients (n=12) and
1075 patients with various cancers other than multiple myeloma (n=5). The lower part of the image
1076 display box plots summarizing the number of CY5 positive cells measured after 14 hours of culture
1077 of twelve multiple myeloma and five non-myeloma bone marrows. C. Effect in MM1s cell
1078 internalization of Cy5 labeled AluSp and its deletion mutants. Images were captured after culturing
1079 cells with the retrotransposons for 8 hours. D. flow cytometry image displaying different degrees of
1080 mCherry expression in cells cultured for 24 hours with AluSp-CMV-mCherry cassette. E. Bar
1081 chart displaying the summary of the number of insertions identified in mCherry expressing (+) and
1082 non-expressing (-) cells. F. Validation of the mCherry integration by PCR from chromatin
1083 extracted from cells treated with AluSp-CMV-mCherry cassette or control-CMV-mCherry
1084 cassette. *nonspecific band. G. Graph displays the confidence of detection of CMV-mCherry
1085 insertions identified versus frequency of each specific site of insertion. H. Cell survival of 3 different
1086 cell lines cocultured with TE-HSV-Tk-GFP for 24 hours prior to adding ganciclovir (GCV).
1087 Apoptosis was measured at 96 hours after GCV addition. MM: multiple myeloma, CC: colon
1088 cancer and PC: pancreatic cancer, TE-CMV-GFP: transposon element joining to CMV-GFP, HSV-
1089 TK: herpes simplex virus thymidine kinase. Error bars in box and whiskers plot identified the
1090 standard deviation of triplicate experiments.

1091

1092 **Figure 6. ctDNA-mediated transmission alters the sensitivity of the cells to bortezomib or**
1093 **gemcitabine.** A. Cell viability assay measuring sensitivity to bortezomib in OPM1 and MM1s
1094 cells cultured with control plasma derived from non-cancer patient or DNase I treated or non-
1095 treated plasma from patients that failed to respond to bortezomib. B. Cell viability assay measuring
1096 sensitivity to bortezomib in RPMI and JK6L cells cultured with control or DNase I-treated or non-
1097 treated plasma from a patient that responded to bortezomib-based treatment. C. Cell viability assay
1098 measuring sensitivity to gemcitabine in pancreatic cancer cell lines (MIA and ASPC-1) cultured
1099 with plasma from patients resistant to gemcitabine, similar plasma pretreated with DNase I or a
1100 control non-cancer patient. For the corresponding DNase I-treated samples, plasma was treated
1101 with DNase I for 10 minutes. D. (Left), Comparison of cell viability response to bortezomib in
1102 OPM1 cells cultured with plasma from a patient that failed to respond to bortezomib treatment,
1103 the combination of control plasma with ctDNA derived from the same patient resistant to

1104 bortezomib and control plasma alone (non-cancer patient). (Middle). Viability response of RPMI
1105 to control plasma or control plasma with added ctDNA obtained from a patient that achieved a
1106 complete response to bortezomib. (Right) Cell viability assessment after bortezomib treatment of
1107 MM1s cells cultured with plasma from a bortezomib resistant patient (BR#2) alone or after
1108 treatment with DNase I or coculture with ctDNA from a different bortezomib-resistant (BR#1)
1109 patient. MM: multiple myeloma and PC: pancreatic cancer. BR: Bortezomib resistant, BS:
1110 Bortezomib sensitive, and GR: Gemcitabine resistant. Error bars indicate the standard deviation of
1111 triplicate experiments.

1112

1113 **Supplemental Figure s**

1114

1115 **Supplemental Figure 1.** A. Agarose gel containing ctDNAs from Multiple myeloma, pancreatic
1116 cancer, and colon cancer ctDNA without or with treatment with Rnase A, DNase I, and proteinase
1117 K. B. Pie chart showing the single nucleotide variants (SNV) shared between tumor from patients
1118 and their corresponding ctDNA (orange) and SNV present only in the tumor sample (blue). C.
1119 GFP expression in MM1s cells cocultured with linearized Cytomegalovirus-green fluorescent
1120 protein: CMV-GFP, ctDNA bound to CMV-GFP, and ctDNA-CMV-GFP. D. ctDNA localization
1121 in tumor xenograft and multiple organs in all ctDNA tail-injected mice. Confocal microscopy of
1122 the xenograft PC tumors harvested from mice after tail injection with rhodamine-PC ctDNA.
1123 Tumors were harvested at 24 and 48 hours post-injection. E. Images of different organs harvested
1124 from xenograft-mice tail injected with rhodamine-ctDNA (MM, CC, and PC) 48 hours after tail
1125 injection (n=3 per tumor xenograft). Images were taken under the red channel to identify
1126 rhodamine fluorescence. MM: multiple myeloma, CC: colon cancer, PC: pancreatic cancer, and
1127 GFP: Green fluorescent protein.

1128 **Supplemental Figure 2.** ctDNA integration into the cell genome. A-B. Visualization images
1129 displaying other examples of the gain of a ctDNA integration into chromatids (red) of CC (HT29
1130 and RKO) and PC (MIA and PANC1) cell lines. Circles define zoomed regions of interest. White
1131 arrows identify an area of ctDNA integration. B. Examples of the metaphase images of various
1132 cancer cell lines (MM1s, ASPC-1, and HT116) treated with ATM, DNAPKcs, PARP, and
1133 transposase inhibitors used to generate Figure 3C. Circles define zoomed regions of interest. White
1134 arrows identify an area of ctDNA integration. C. Cell viability assays of MM1, ASPC1, and

1135 HTC116 cells after 24 hours treatment with 100 nM of ATM inhibitor (KU-55933), 30 mM of
1136 DNAPKcs Inhibitor II, 200 mM of PARP inhibitor (NU1025) or 100nM of raltegravir. PC:
1137 Pancreatic cancer and CC: Colon cancer. MM1s: Myeloma cell line.

1138 **Supplemental Figure 3.** A. Visualization images displaying other examples of the gain of a
1139 ctDNA SNV in the coculture experiment. B. Blast images demonstrate the transition point of a
1140 ctDNA insertion event in multiple myeloma or pancreatic cancer coculture when compared to the
1141 cell line and ctDNA contigs. Green boxes reflect cell genome contigs, and red boxes reflect ctDNA
1142 contigs. Coculture Contigs carrying and insertion were identified using NucDiff analysis.

1143 **Supplemental Figure 4.** Gene ontology analysis demonstrates the processes and pathways
1144 enriched in the matching coculture conditions. Gene ontology processes include biological,
1145 molecular function, and cellular functions.

1146 **Supplemental Figure 5.** A. PCR of the Control- or all transposons performed from DNA extracted
1147 after culturing these constructs with complete media for 4 hours. B. Time course of Cy5-AluSp
1148 and -control sequence treated MM1s cells (1 μ g/mL). CY5(+) cells were detected by flow
1149 cytometry. C. Dose titration experiments of Cy5-AluSp and -control sequence treated MM1s cells.
1150 Before flow cytometry, half of the samples were treated with trypsin to identify how much DNA
1151 was internalized. D. flow cytometric screening of all transposons and controls in U266 cells after
1152 4 hours in culture. E. Graphical display of the adenine (A)-thymine (T) and guanine (G)-cytosine
1153 (C) enrich regions or both. F. Consensus sequences from all MM retrotransposons were obtained
1154 after multiple alignments using EMBOSS Cons software. G. Microscopy images of MM1s cells
1155 cultured with AluSp-CMV-mCherry, CMV-mCherry linear vector or cells transfected with CMV-
1156 mCherry circular vector. Images were captured after 24 hours of coculture with DNA.

1157

1158 **Supplemental Table and Video Legends**

1159

1160 **Supplemental Table 1.** Table summarizing the distribution of the contigs containing transposons
1161 and the fraction of transposons observed at 5' or 3' end in inserted *vs.* non inserted ctDNA
1162 fragments.

1163 **Supplemental Table 2.** Table summarizing the number of contigs containing a specific class and
1164 type of TE in all inserted and non-inserted contigs in MM and PC coculture experiments. Statistical
1165 analysis was performed using the Chi-square test. Significance was determined on the basis of a
1166 p-value of <0.05. MM: multiple myeloma, PC: pancreatic cancer.

1167

1168 **Supplemental Spreadsheet 1.** Summary of the chromosomal location of origin and insertion and
1169 their frequency in the MM (A) and PC (B) coculture experiment. CHR: chromosome. MM:
1170 multiple myeloma, PC: pancreatic cancer

1171

1172 **Supplemental Video 1A and B.** Rotational images of 3D reconstruction of cellular and nuclear
1173 capture of rhodamine-labeled PC ctDNA in ASPC1 cells (B) and MM ctDNA in MM1s (A).
1174 Images show cellular localization of ctDNA. Membrane identified by bright field (gray color) and
1175 ctDNA (yellow color).

1176

1177 **Supplemental Video 2. A.** Slide image of ASPC1 demonstrating the capturing and nuclear
1178 localization of rhodamine-labeled PC ctDNA. **B.** Different slices of Z-stack images ASPC1 cells
1179 demonstrating ctDNA capturing in the cell membrane and invagination of cell membrane for
1180 internalization of ctDNA. **C.** 3D video reconstruction of B. Cell membrane was labeled using
1181 CellLight Plasma Membrane GFP kit (ThermoFisher Scientific, MA)

1182

1183 **Supplemental Video 3 A and B.** 3D reconstruction of colocalization of match (rhodamine – Red)
1184 and unmatched (CY5 – green) ctDNA coculture with MM1s cells.

Figure 1

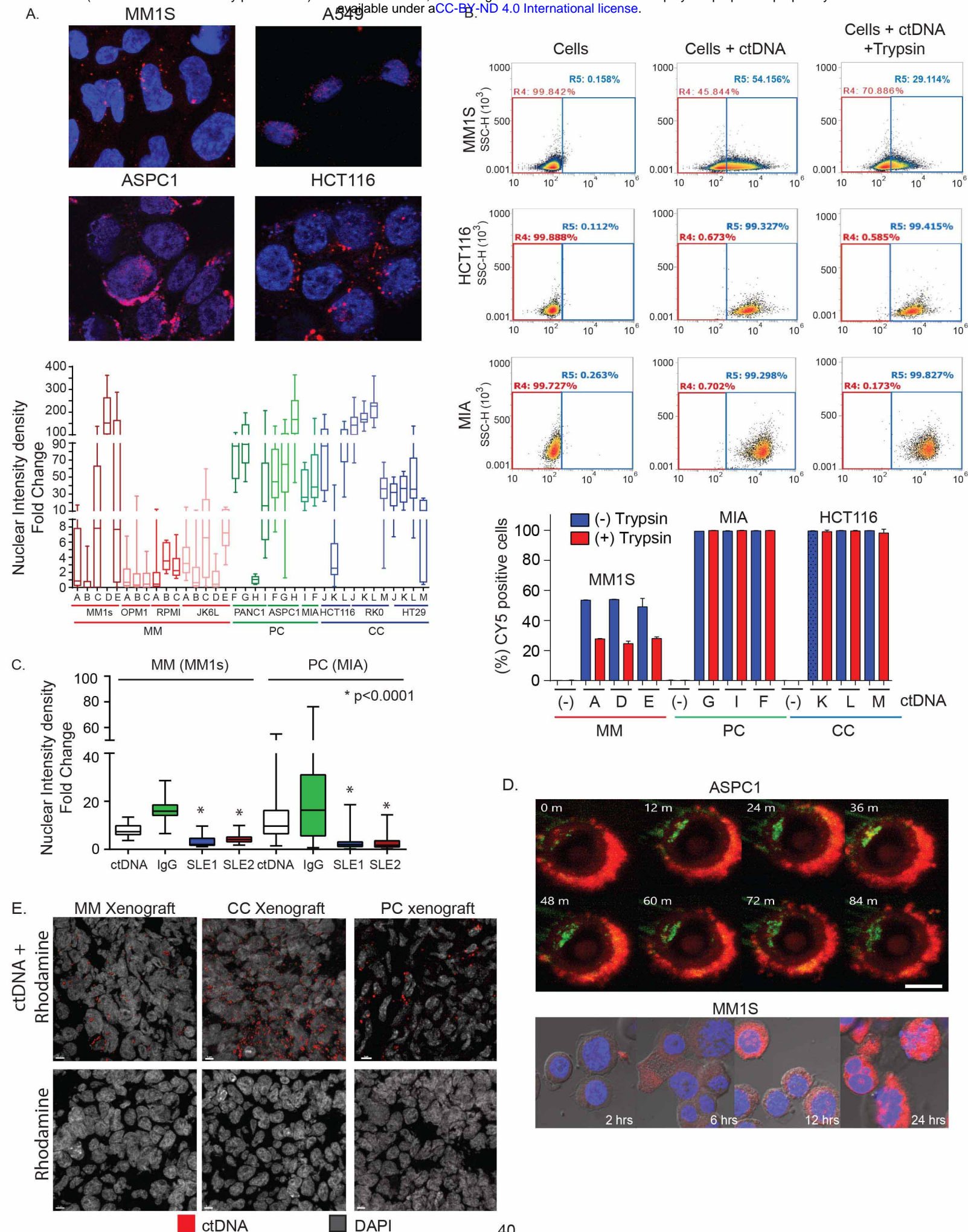
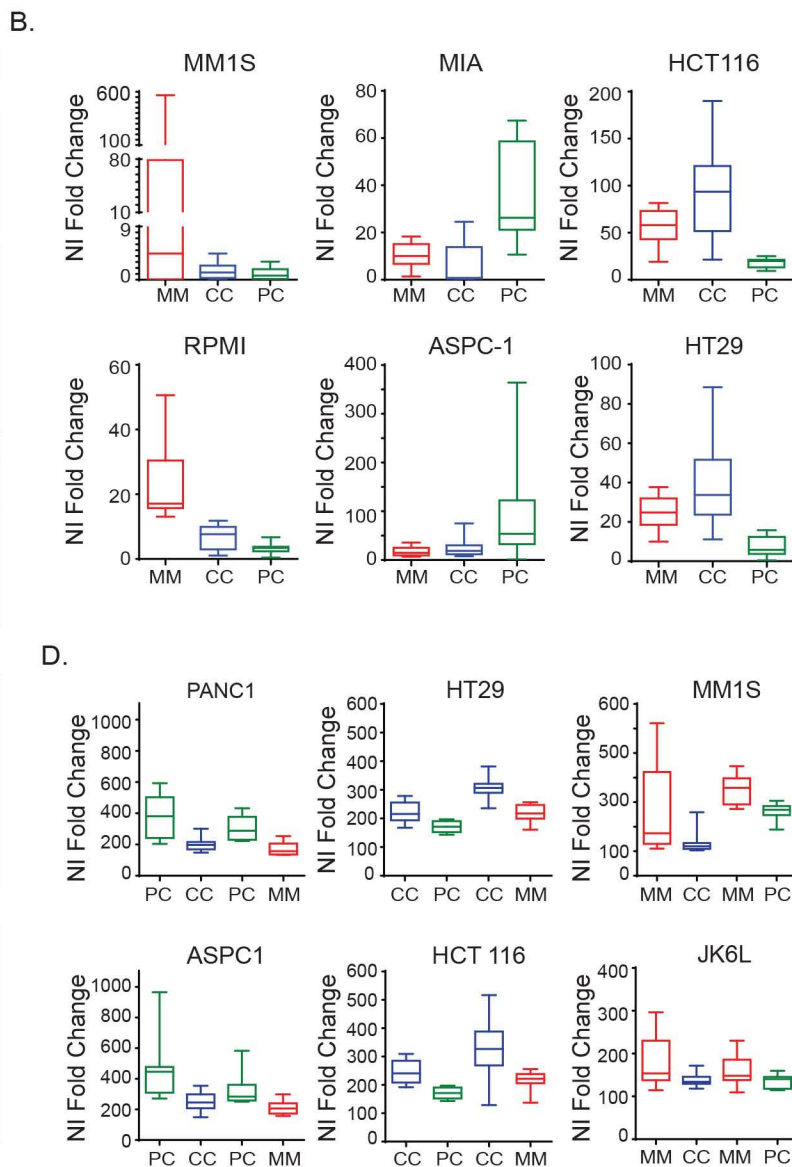
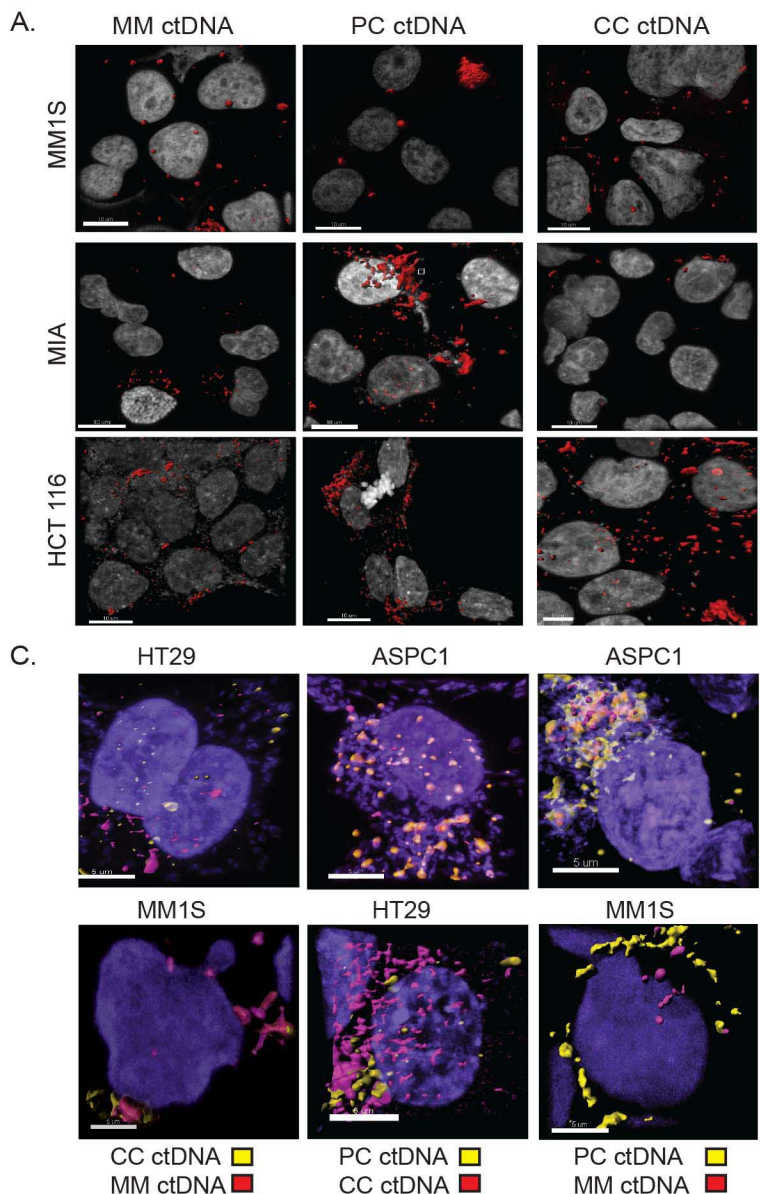
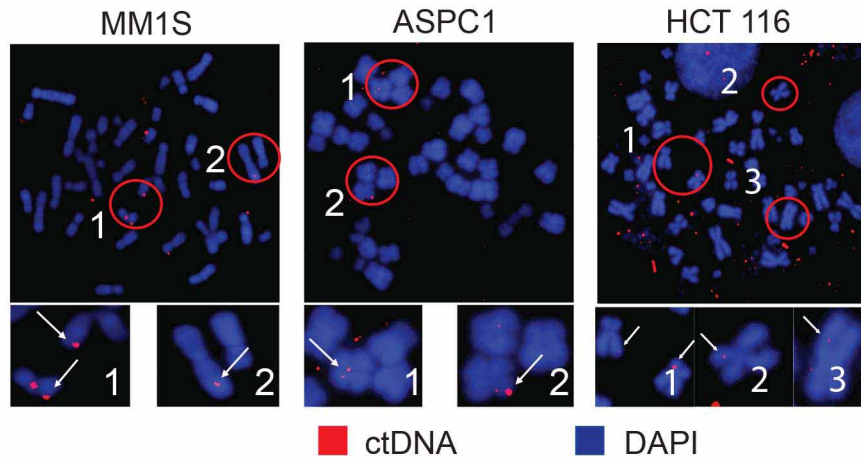


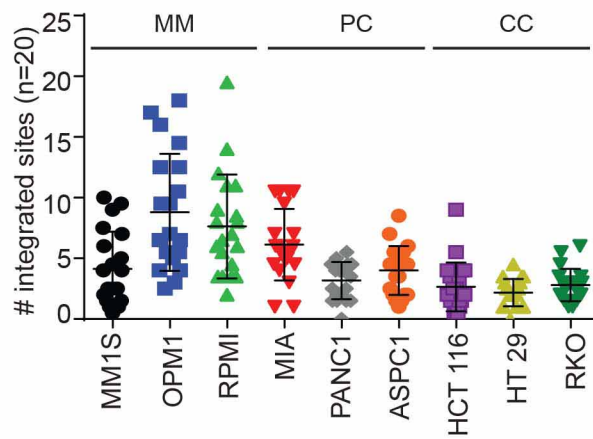
Figure 2



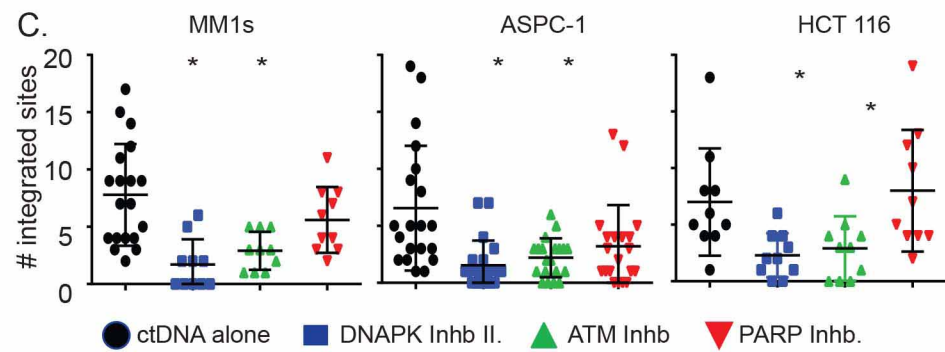
A.



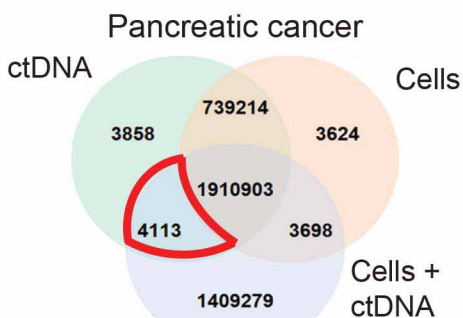
B.



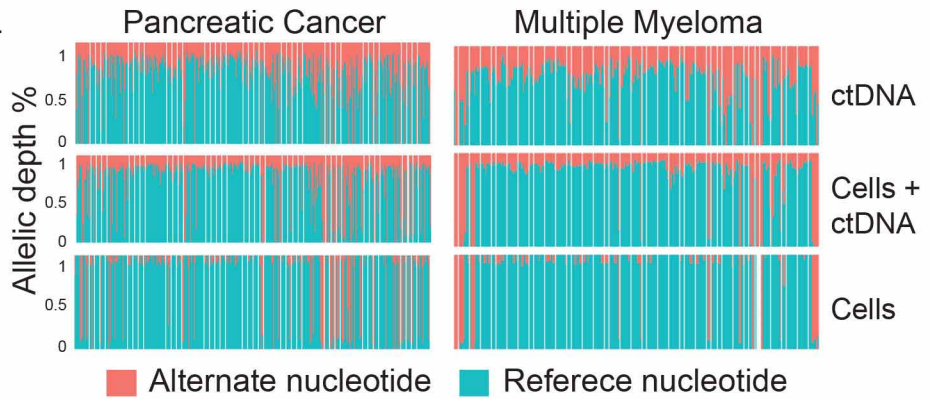
C.



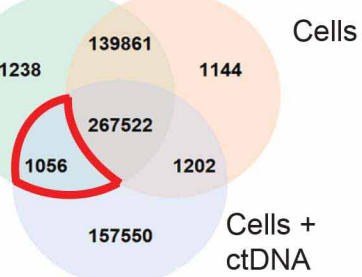
D.



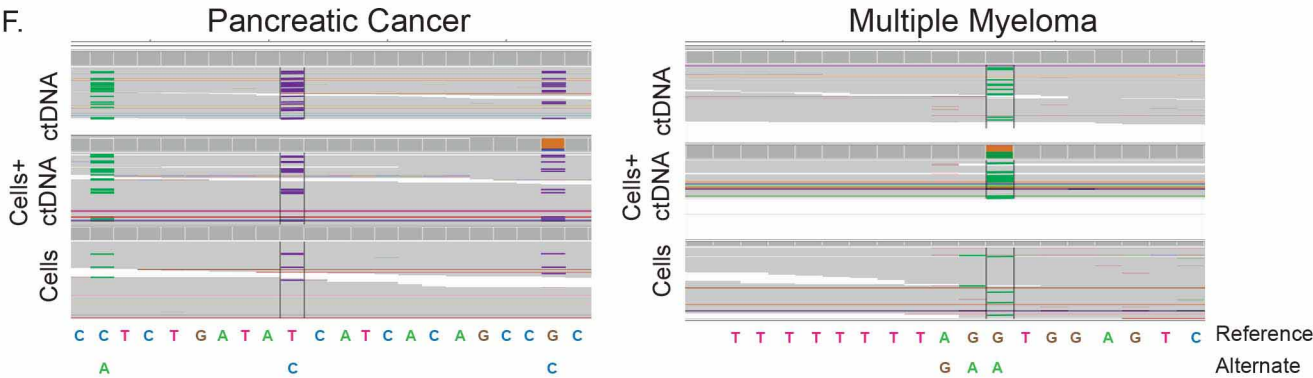
E.



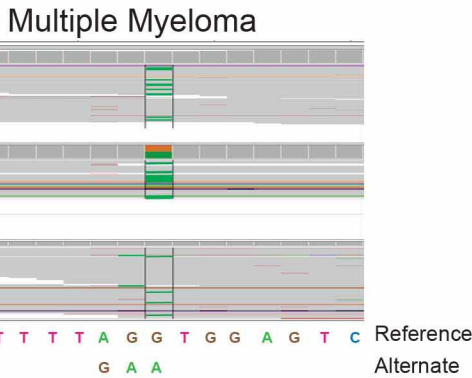
Pancreatic cancer



F.



Pancreatic Cancer



G.

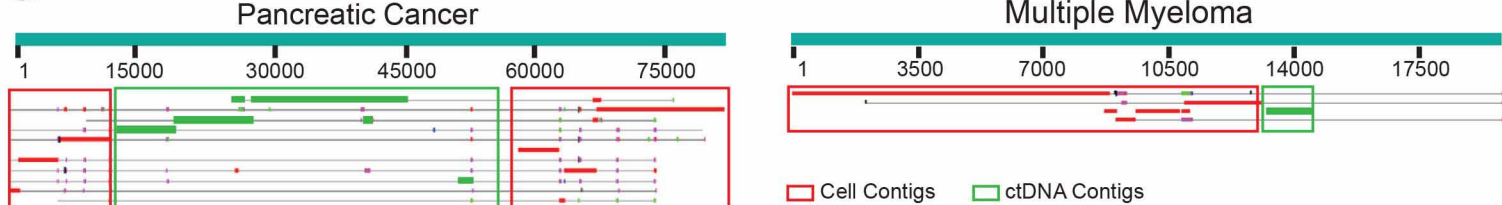


Figure 4

A.

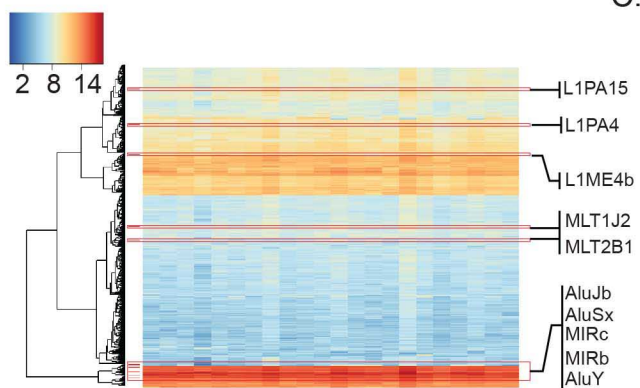
Multiple Myeloma

Repeat Family	Class	Geomic Position
AluSp	SINE	chr16:32628455-32628757
AluSq	SINE	chr2:86528424 - 86530643
L1MB3	LINE	chr2:86530293-86531176
THE1C	ERVL	chr14: 32672352-32670273
MER11C	ERVK	chr14: 46404852- 46401883
AluY	SINE	chr13: 22562455- 22559956

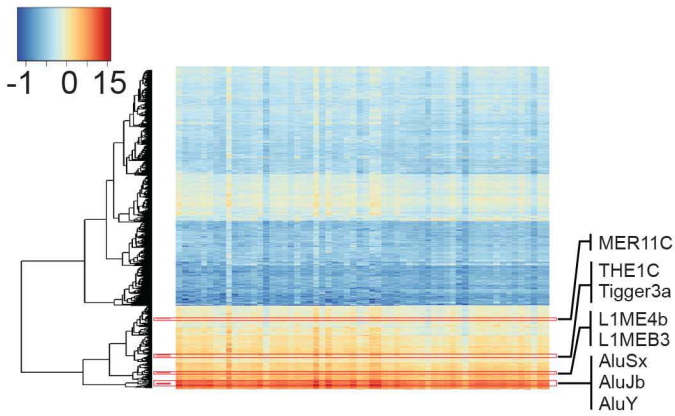
Pancreatic Cancer

Repeat Family	Class	Geomic Position
AluSx	SINE	chr20:60038954-60039263
AluJb	SINE	chr7:78205135-78205431
MLT2B4	ERVL	chr3:128760021-128760429
L2a	LINE	chr21:39058193-39058285
MLT1J2	ERVL	chr21:39058684-39058826
AluSp	SINE	chr3:128759714-128760009

B.



C.



D.

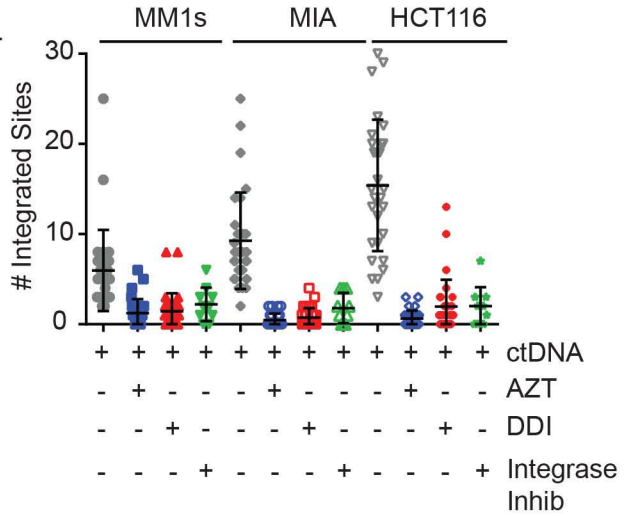
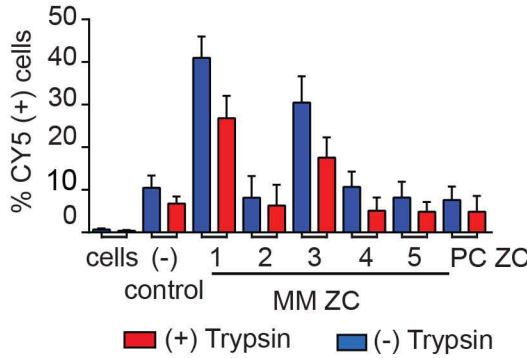
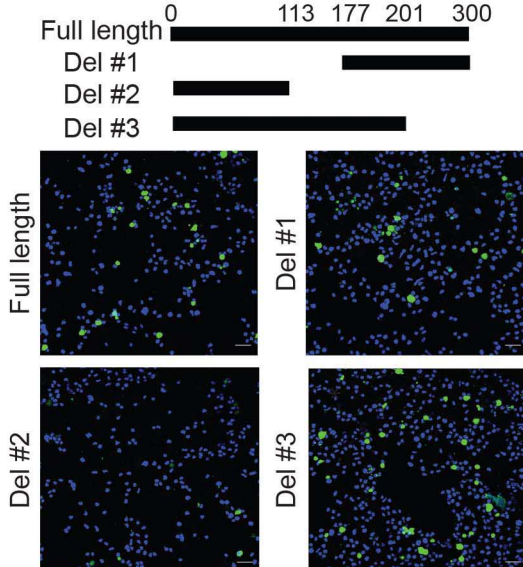


FIGURE 5.

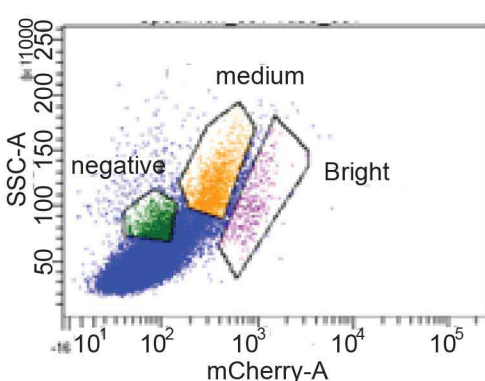
A.



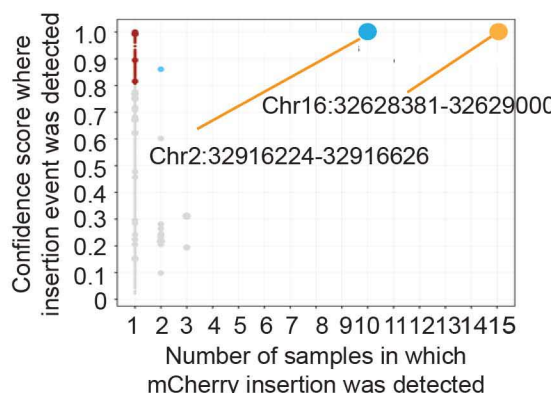
C.



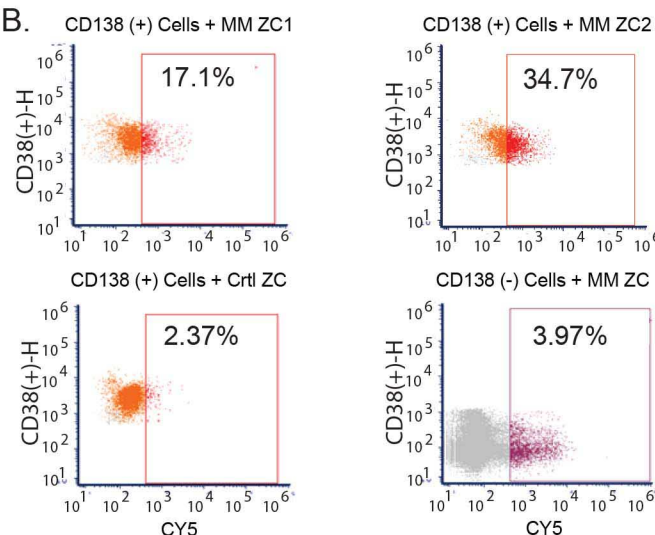
D.



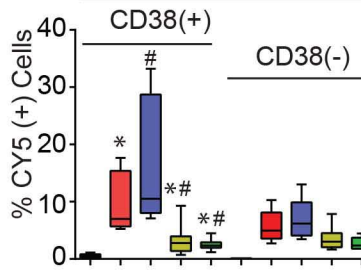
G.



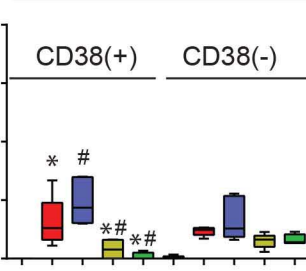
B.



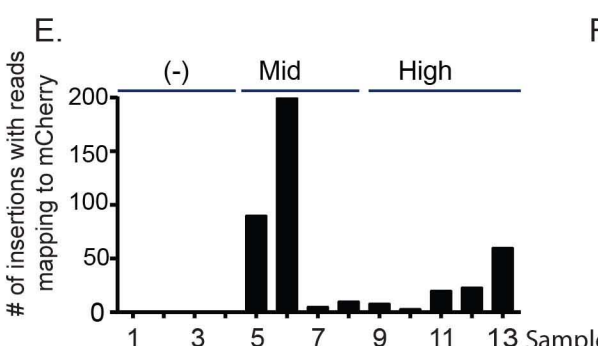
Multiple Myeloma



Normal BM



E.



F.



H.

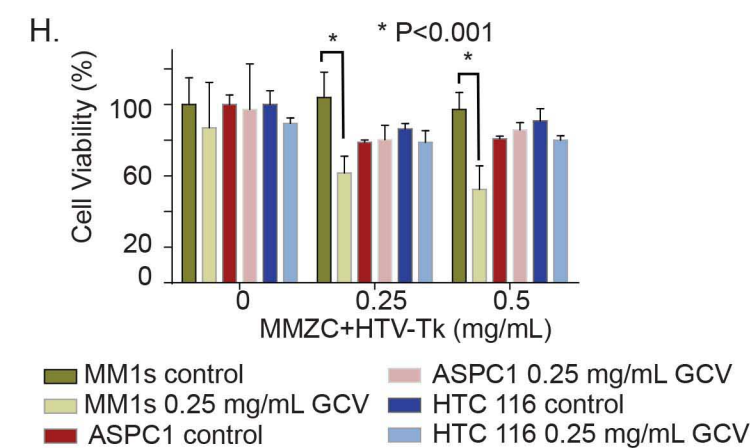


Figure 6

